NASA
Technical
Paper
2391

February 1985

Static Internal Performance of a Two-Dimensional Convergent Nozzle With Thrust-Vectoring Capability up to 60°

Laurence D. Leavitt

NASA

NASA Technical Paper 2391

1985

Static Internal Performance of a Two-Dimensional Convergent Nozzle With Thrust-Vectoring Capability up to 60°

Laurence D. Leavitt

Langley Research Center
Hampton, Virginia

NASA
National Aeronautics
and Space Administration

Scientific and Technical Information Branch

Summary

An investigation has been conducted at wind-off conditions in the static-test facility of the Langley 16-Foot Transonic Tunnel to determine the internal performance characteristics of a two-dimensional convergent nozzle with a thrust-vectoring capability up to 60°. Vectoring was accomplished by a downward rotation of a hinged upper convergent flap and a corresponding rotation of a center-pivoted lower convergent flap. The effects of geometric thrust-vector angle and upper-rotating-flap geometry on internal nozzle performance characteristics were investigated. Nozzle pressure ratio was varied from 1.0 (jet off) to approximately 5.0.

Results of the investigation indicate that unvectored performance of the two-dimensional convergent nozzle was comparable to unvectored axisymmetric nozzle levels. The nozzle was, in general, highly effective in providing large thrust-vector angles (up to 60°) with little loss in resultant thrust ratio.

Introduction

Increased mission requirements for tactical aircraft have given rise to the consideration of propulsion system participation in the enhancement of aircraft maneuver, attitude control, and take-off and landing performance. Propulsion systems in which the nozzles have the ability to change the direction of the thrust vector to generate forces and moments have been considered. If such a propulsion system were incorporated properly into the aircraft system, significant performance improvements could be realized. Both axisymmetric (refs. 1 to 5) and nonaxisymmetric nozzle configurations (refs. 1 and 5 to 24) have been examined; however, the nonaxisymmetric (two-dimensional) nozzle has been found to be much more amenable to incorporation of thrust-vectoring schemes (ref. 23).

To date, most of the research on vectoring nonaxisymmetric nozzle internal performance has been conducted on either the single-expansion-ramp nozzle (SERN) (refs. 4, 6, and 9 to 23) or the two-dimensional convergent-divergent (2-D C-D) nozzle (refs. 1, 4, 5, 7, 8, 11 to 16, 19, 21, and 23 to 25). Thrust vectoring on SERN nozzles is accomplished by several different mechanical schemes, but on 2-D C-D nozzles most of the vectoring schemes depend on rotation of the divergent flaps to turn the nozzle flow. When a convergent two-dimensional nozzle is considered, some other method of nozzle actuation to vector thrust must be examined since divergent flaps are not present on a convergent nozzle.

The present paper contains static internal performance data and a limited amount of internal pressure distribution data for a nonaxisymmetric convergent nozzle that was originally designed in a program to examine the incorporation of thrust vectoring (for providing STOL capability) into the Grumman A-6 aircraft. The A-6 aircraft is amenable to the incorporation of thrust vectoring, because the exhaust nozzles are near the aircraft center of gravity. Hence, extensive redesign of tail surfaces or addition of canards to trim the thrust vector would be unnecessary. The data are intended to help provide an understanding of the complex flow mechanisms involved in vectoring a convergent nozzle to provide resultant thrust angles significantly higher than previously considered (up to 60°) as well as to extend the current data base on nonaxisymmetric nozzles. The nozzle investigated was a unique concept, in that vectoring was accomplished by the downward rotation of a hinged upper convergent flap and a corresponding rotation of a center-pivoted lower convergent flap. The effects of thrust-vector angle and upper-rotating-flap geometry on internal nozzle performance characteristics were investigated for nozzle pressure ratios from 1.0 (jet off) to approximately 5.0.

Symbols

All forces (with the exception of resultant gross thrust) and angles are referred to the model centerline (body axis). A detailed discussion of the data-reduction and calibration procedures as well as definitions of forces, angles, and propulsion relationships used herein can be found in reference 21.

A_t	total nozzle throat area, in^2
F	measured thrust along body axis, lbf
F_i	ideal isentropic gross thrust, $w_p\sqrt{\frac{RT_{t,j}}{g}\left(\frac{2\gamma}{\gamma-1}\right)\left[1-\left(\frac{p_a}{p_{t,j}}\right)^{\frac{\gamma-1}{\gamma}}\right]}$, lbf
F_r	resultant gross thrust, $\sqrt{F^2+N^2}$, lbf
g	gravitational constant, 32.174 ft/sec^2
h_l	secondary-nozzle throat height (fig. 3(b)), in.
h_u	primary-nozzle throat height (fig. 3(b)), in.
$l_{l,\text{fixed}}$	length of lower fixed flap, 1.300 in.
$l_{l,\text{rot}}$	length of lower rotating flap, 2.690 in.
$l_{u,\text{rot}}$	length of upper rotating flap, 1.397 in.
N	measured normal force, lbf

NPR	nozzle pressure ratio (ratio of jet total pressure to ambient pressure)
p	local static pressure, psi
p_a	ambient pressure, psi
$p_{t,j}$	jet total pressure, psi
R	gas constant for air, 53.364 ft-lb/lb°R
$T_{t,j}$	jet total temperature, °R
w_i	ideal weight-flow rate, lbf/sec
w_p	measured weight-flow rate, lbf/sec
x	axial distance measured from nozzle connect station, positive downstream, in.
x'	location of upper-flap pressure orifices on longitudinal axis which rotates (with upper rotating flap), is parallel to internal surface of baseline upper rotating flap, and is positive downstream of hinge point of upper rotating flap. Negative x' is parallel to body axis and remains fixed (fig. 3(a)), in.
x''	chordwise location of pressure orifices on lower rotating flap, positive downstream of leading edge of lower rotating flap (fig. 3(a)), in.
z	vertical distance measured from model centerline, positive up, in.
γ	ratio of specific heats, 1.3997 for air
δ	measured resultant thrust-vector angle, $\tan^{-1}\frac{N}{F}$, deg
δ_l	lower-flap rotation angle (fig. 3(a)), positive down, deg
δ_u	upper-flap rotation angle (fig. 3(a)), positive down, deg
δ_v	design thrust-vector angle measured from horizontal reference line, positive down, deg

Sidewall orifice designations:

PRSID1 to PRSID37	sidewall static pressures (tables II to XVI and fig. 3(d))

Abbreviations:

Conf	configuration
rot	rotating
Sta.	model station, in.

Apparatus and Methods

Static-Test Facility

This investigation was conducted in the static-test facility of the Langley 16-Foot Transonic Tunnel with the jet exhausting to atmosphere. This facility utilizes the same clean, dry-air supply as that used for jet simulation in the Langley 16-Foot Transonic Tunnel and a similar air-control system —including valving, filters, and a heat exchanger (to operate the jet flow at constant stagnation temperature).

Single-Engine Propulsion Simulation System

A sketch of the single-engine air-powered nacelle model on which various nozzles were mounted is presented in figure 1 with a typical nozzle configuration attached. The body shell forward of station 20.50 was removed for this investigation.

An external high-pressure air system provided a continuous flow of clean, dry air at a controlled temperature of about 530°R. This high-pressure air was brought through a dolly-mounted support strut by six tubes which connect to a high-pressure plenum chamber. As shown in figure 1, the air was then discharged perpendicularly into the model low-pressure plenum. This method was designed to minimize any forces imposed by the transfer of axial momentum as the air is passed from the nonmetric high-pressure plenum to the metric (mounted to the force balance) low-pressure plenum. Two flexible metal bellows are used as seals and serve to compensate for axial forces caused by pressurization. The air was then passed from the model low-pressure plenum (circular in cross section) through a transition section, a choke plate, and an instrumentation section. The transition section provided a smooth flow path for the airflow from the round low-pressure plenum to the rectangular choke plate and instrumentation section. The instrumentation section had a flow path width-height ratio of 1.437 and was identical in geometry to the nozzle airflow entrance. The nozzles were attached to the instrumentation section at model station 41.13.

Nozzle Design

Figure 2(a) is a photograph of a typical nonaxisymmetric nozzle installed on the single-engine propulsion system. Photographs of typical vectored and unvectored nozzle configurations with one sidewall removed are shown in figure 2(b). As seen in the photographs and in the model sketches presented in figure 3, the nozzle is a nonaxisymmetric convergent nozzle in the

forward thrust mode ($\delta_v = 0°$). Thrust vectoring up to $\delta_v = 60°$ was accomplished by a downward rotation of a hinged upper flap and a corresponding rotation of a center-pivoted lower flap. (See fig. 2(b).) At $\delta_v = 0°$, the nozzle throat is fixed at the nozzle exit. For $\delta_v > 0°$, the nozzle has two separate throats—one between the upper rotating flap and the top surface of the lower rotating flap and one between the bottom surface of the lower rotating flap and the fixed segment of the lower flap. This type of vectoring scheme can be advantageous in that the center of action of the resultant thrust vector is farther upstream (closer to the airplane center of gravity) than would be expected for a more typical thrust-vectoring scheme, for which two hinged flaps are rotated downward simultaneously.

Important configuration parameters for the configurations investigated are shown in table I and details of the model geometry are shown in figure 3. For all vectored configurations, the lower-flap rotation angle δ_l is equal to the design thrust-vector angle δ_v. The upper-flap rotation angle δ_u increased as nozzle δ_v increased except for the $\delta_v = 60°$ configurations. As shown in table I, for a design thrust-vector angle of 60°, the rotation angle for the upper flap lies between those values indicated for vector angles of 15° and 30°. The upper-flap rotation angles were selected to provide a nearly constant effective flow area independent of thrust-vector angle. Effective flow area could be expressed as the product of discharge coefficient w_p/w_i and measured total throat area A_t. Thus, in anticipation of a large drop in discharge coefficient at $\delta_v = 60°$, upper throat area was increased by decreasing upper-flap rotation angle at $\delta_v = 60°$. Measured total throat area tends to increase with increasing design thrust-vector angle (see table I) for the model hardware investigated.

In addition to geometric thrust-vector angle, the geometry of the upper rotating flap was investigated. Sketches of the three geometries tested are shown in figure 3(c). The angled upper rotating flap was identical in length to the baseline flap, but the flap surface was modified to provide an 8.05° increase in the terminal angle of the upper rotating flap. This modification was used to determine what effects, if any, terminal angle had on overall nozzle turning characteristics. The long upper rotating flap was merely an extended baseline flap (0.5 in. longer) and was expected to provide larger turning angles than the baseline flap, because flow is contained longer on the upper surface of the lower rotating flap. The sidewall extension shown in figure 3(d) was used to provide full sidewall containment on those configurations employing the long upper rotating flap.

For purposes of discussion, the exhaust flow path formed between the upper rotating flap and the top surface of the lower rotating flap is referred to as the primary exhaust passage. The exhaust flow path between the bottom surfaces of the lower rotating flap and the lower fixed flap is referred to as the secondary exhaust passage.

Instrumentation

A three-component strain-gauge balance was used to measure the forces and moments on the model downstream of station 20.50 in. (See fig. 1.) Jet total pressure was measured at a fixed station in the instrumentation section (see fig. 1) by means of a four-probe rake through the upper surface, a three-probe rake through the side, and a three-probe rake through the corner. A thermocouple, also located in the instrumentation section, was used to measure jet total temperature. Weight-flow rate of the high-pressure air supplied to the nozzle was determined from pressure and temperature measurements in the high-pressure plenum (located on top of the support strut) calibrated with standard axisymmetric nozzles of known discharge coefficient. Internal static-pressure orifices were located on all fixed- and rotating-flap hardware tested and on the right-hand sidewall. The static-pressure orifices located on the nozzle flaps (both fixed and rotating) consisted of a single row of orifices along the centerline. Actual locations of these orifices can be determined by examination of tables II to XVI. Static-pressure orifice locations on the sidewalls are shown in figure 3(d). Because of the rotating geometry, three independent axis systems were used to define static-pressure orifice locations. The symbols x' and x'' represent axis systems used to locate pressure orifices on the upper flap (rotating and fixed segments) and on the lower rotating flap, respectively. (See fig. 3(a).) The symbol x represents an axis system which is parallel to the model body axis and positive downstream of the nozzle connect station. It is used to locate pressure orifices on the sidewall (see fig. 3(d)) and on the fixed lower flap (see fig. 3(a)). The positive x' axis is defined to be parallel to the internal surface of the baseline upper rotating flap and is positive downstream of the upper rotating flap pivot point located at model station 43.58. (See fig. 3(a).) The negative x' axis is parallel to the body axis and remains fixed. The axis system labeled x'' is defined to be parallel to the lower rotating flap centerline and positive downstream of the rotating flap leading edge. Both the positive x' and x'' axes rotate with δ_u and δ_l, respectively. Pressure orifice locations were defined in this manner to allow a more direct comparison of the respective upper and lower rotating flap pressure distributions.

Data Reduction

All data were recorded simultaneously on magnetic tape. Approximately 50 frames of data, taken at a rate of 10 frames per second, were used for each data

point; average values were used in computations. Data were recorded in an ascending order of $p_{t,j}$. With the exception of resultant gross thrust F_r, all force data in this report are referenced to the model centerline.

The basic performance parameters used for the presentation of results are F/F_i, F_r/F_i, δ, and w_p/w_i. The internal thrust ratio F/F_i is the ratio of actual nozzle thrust (along the body axis) to ideal nozzle thrust, with ideal nozzle thrust based on measured weight-flow rate and total temperature and pressure conditions in the nozzle throat as defined in the symbols. The balance axial-force measurement, from which actual nozzle thrust is subsequently obtained, is initially corrected for model weight tares and balance interactions. Although the bellows arrangement was designed to eliminate pressure and momentum interactions with the balance, small bellows tares on axial, normal, and pitch balance components still exist. These tares result from a small pressure difference between the ends of the bellows when internal velocities are high and from small differences in the forward and aft bellows spring constants when the bellows are pressurized. As discussed in reference 21, these bellows tares were determined by running calibration nozzles with known performance over a range of expected normal forces and pitching moments. The balance data were then corrected in a manner similar to that discussed in reference 21 to obtain actual nozzle thrust, normal force, and pitching moment. The resultant gross thrust F_r, used in resultant thrust ratio F_r/F_i, and the measured resultant thrust vector angle δ are then determined from these corrected balance data. Resultant thrust ratio F_r/F_i is equal to internal thrust ratio F/F_i as long as the jet-exhaust flow remains unvectored ($\delta = 0°$). Significant differences between F_r/F_i and F/F_i occur when jet exhaust flow is turned from the axial direction; the magnitudes of these differences are a function of δ. Nozzle discharge coefficient w_p/w_i is the ratio of measured weight-flow rate to ideal weight-flow rate with ideal weight-flow rate based on jet total pressure $p_{t,j}$, jet total temperature $T_{t,j}$, and measured nozzle throat area.

Presentation of Results

The results of this investigation are plotted in the following figures:

Discussion of Results

Internal Static-Pressure Distributions

Internal static-pressure-ratio $p/p_{t,j}$ data are presented in tabulated form in tables II to XVI for each nozzle pressure ratio (NPR) and configuration tested. Static-pressure-ratio data are presented for all orifice locations and include pressure for both upper and lower flaps as well as for the nozzle sidewall. Typical internal static-pressure-ratio distributions for various configuration comparisons are shown in figures 4 to 6.

Effects of vector angle on lower-rotating-flap pressures. The effects of thrust-vector angle on lower-rotating-flap centerline static-pressure distributions are presented in figure 4 for all three upper-rotating-flap configurations tested. Pressures on both the top and bottom surfaces of the lower rotating flap are shown for a nominal NPR of 3.0.

As seen in figure 4, static pressures on the top surface of the lower rotating flap generally decreased as thrust-vector angle increased from 15° to 60°. The 45° and 60° vectoring cases exhibit pressure distribution characteristics which are significantly different from those of the 15° and 30° vectoring cases and are similar in character to distributions observed for single-expansion-ramp nozzles (SERN). Reasons for these differences are discussed in more detail subsequently.

Static pressure generally increased on the bottom surface of the lower-rotating-flap as thrust-vector angle increased in all cases except at $\delta_v = 15°$. At this thrust-vector angle, the throat height of the secondary exhaust passage h_l is small relative to the exit height (formed by the lower rotating flap and the termination of the fixed lower-flap radius). Therefore, there is a relatively large secondary-passage expansion ratio (ratio of exit area to throat area). Since the NPR required for fully expanded flow (design NPR) is much higher than NPR = 3.0 for a large expansion ratio, the secondary exhaust passage is greatly overexpanded. The static-pressure-ratio distributions shown for $\delta_v = 15°$ reflect this fact and indicate shock-induced separation over the last 50 percent of the bottom surface of the lower rotating flap. This shock-induced separation is generally characterized by a sudden increase in pressure followed by a "plateau" or region of little change in pressure. With such a large separated region, nozzle thrust performance would be expected to suffer. Of course, as NPR is increased, these shock-induced-separation losses should decrease and result in increased nozzle performance in the secondary passage. Unfortunately, the primary-nozzle passage at $\delta_v = 15°$ forms a convergent

nozzle with a design NPR of approximately 2.0; hence, increases in the performance of the secondary-nozzle passage may be more than offset by increased underexpansion losses (NPR > design NPR) in the primary passage as NPR is increased.

As might be expected with the large variations in static-pressure distributions shown in figure 4, geometric thrust-vector angle also had a large impact on throat location ($p/p_{t,j} = 0.528$), especially on the lower rotating flap. As δ_v increased, the throat location moved upstream on the top surface of the lower rotating flap and downstream on the bottom surface of the lower rotating flap. These shifts in throat location have a large effect on the length of the external expansion surface (expansion occurring downstream of the nozzle exit) and are at least in part responsible for the fact that these data exhibit some similarity to SERN static-pressure distributions. (See refs. 19, 20, 22, and 24.) This was especially true at the higher geometric thrust-vector angles (45° and 60°). Very often, SERN static-pressure distributions on the ramp are characterized by a pattern of alternate regions of expansion and compression. Examination of model geometry (e.g., see fig. 3(b)) indicates that the lower rotating flap becomes an external expansion surface aft of the exit planes of both the primary and secondary exhaust passages during vectored-thrust operation.

For the $\delta_v = 60°$ configurations, it is seen in figures 4(a) and (b) that the initial extreme overexpansion downstream of the throat on the top surface is followed by a compression (increased pressures), an expansion (decreased pressures), and another compression (which may be a weak shock near the trailing edge of the lower rotating flap). The SERN-like trends are more predominant at the higher thrust-vector angles because the upstream movement of the throat in the primary exhaust passage results in a relative increase in the exposed length of the external expansion surface as thrust-vector angle increases.

Effects of vector angle on upper-flap pressures. The effects of thrust-vector angle on upper-flap centerline static-pressure distributions are presented in figure 5. In all cases except $\delta_v = 60°$ with the long upper rotating flap installed (fig. 5(c)), static-pressure ratios were higher for vectored nozzle configurations than for unvectored configurations. For thrust-vector angles from 15° to 45°, variations in static-pressure distributions for changes in vector angle were very small. The location of the nozzle throat ($p/p_{t,j} = 0.528$) was downstream of the last orifice on the upper rotating flap (except for the long upper rotating flap at $\delta_v = 60°$). This location indicated subsonic flow up to the nozzle exit. Several studies (summarized in ref. 23) have concluded that subsonic turning of the exhaust flow results in fewer turning losses; hence, reasonably high primary exhaust passage performance might be expected. The $\delta_v = 60°$ configurations resulted in static pressures on the upper rotating flap for all three upper-rotating-flap configurations which were lower than those for the other vectored configurations tested. As discussed previously in the "Nozzle Design" section, the upper rotating flap was not rotated downward as much for the $\delta_v = 60°$ configurations as for the $\delta_v = 30°$ and 45° configurations. As a result, the primary exhaust passage convergence is decreased relative to the $\delta_v = 30°$ and 45° configurations, and for the case of the long upper rotating flap, some primary-passage divergence actually occurs. The net result is an overall decrease in the static pressure on the upper rotating flap.

Effects of vector angle on lower-flap fixed-segment pressures. The effects of design thrust-vector angle on static-pressure-ratio distributions of the fixed segment of the lower flap are presented in figure 6 for the baseline upper rotating flap. Data are presented only for the baseline upper rotating flap, because lower fixed-flap static pressures were independent of the upper rotating flap configuration. Once the secondary exhaust passage was opened ($\delta_v > 0°$), pressures on the lower fixed flap decreased, and throat location moved upstream as δ_v increased up to 30°. Additional increases in thrust-vector angle had little effect on throat location. Of course, only the primary throat exists when the secondary exhaust passage is closed ($\delta_v = 0°$).

Effects of upper-rotating-flap configuration. The effects of upper-rotating-flap configuration on static-pressure-ratio distributions of the lower rotating flap can be examined by comparison of figures 4(a) to (c). Pressure distributions on the bottom surface are relatively independent of upper-rotating-flap configuration. Upper-flap exit terminal angle had almost no effect on static pressures on the top surface of the lower rotating flap, but static pressures were generally somewhat higher for the long upper rotating flap.

Comparison of figures 5(a) to (c) indicates that increased convergence (relative to the baseline) resulting either from a steeper terminal angle (as on the angled upper rotating flap) or from increased length of the converging region (as on the long upper rotating flap), caused an increase in static pressures on the rotating segment of the upper flap. Again, the 60° vectoring case is the exception.

Contours of $p/p_{t,j}$. Contours of sidewall $p/p_{t,j}$ for several nozzle configurations are presented in figure 7. These contours were computed using a very limited number of pressures (see fig. 3(d)) and should be used only as a qualitative indication of internal flow properties. The pressures used for the contours consisted of the entire series of static sidewall and upper- and lower-flap centerline static pressures where needed

to represent a reasonable contour. Thus, it was assumed that the flap centerline static pressures were uniform across the entire flap width. It must be cautioned, however, that a substantial nonuniform, three-dimensional flow field can exist, especially in the throat region, as discussed in reference 25. Straight and Cullom (ref. 25) report that sidewall static pressures in the throat region tend to remain higher than flap static pressures at a given axial station.

Contours of $p/p_{t,j}$ for all three upper-rotating-flap configurations are presented in figures 7(a) to (c) for $\delta_v = 0°$. As discussed previously, internal static pressures at a given axial location in the nozzle were somewhat higher for the angled and long upper rotating flap than for the baseline upper rotating flap. In all cases, the pressure distributions were uniform.

The remaining contour plots of $p/p_{t,j}$ are for the range of thrust-vector angle tested with the baseline upper rotating flap and are presented in figures 7(d) to (g). For $\delta_v = 15°$, the contour plot shown in figure 7(d) indicates, as discussed previously, highly expanded flow in the secondary exhaust passage and subsonic flow up to the nozzle exit in the primary nozzle passage. As expected, the secondary-passage throat ($p/p_{t,j} = 0.528$) is formed near the leading edge of the lower rotating flap. Increases in the thrust-vector angle to 30° or higher result in relatively uniform flow in the secondary nozzle passage. (See figs. 7(e) to (g).) As the lower rotating flap angle δ_l increases, throat location on the bottom surface of the lower rotating flap moves downstream, and the throat appears to be more or less perpendicular to the lower rotating flap. As was the case for $\delta_v = 15°$, both the $\delta_v = 30°$ and $\delta_v = 45°$ configurations indicate subsonic flow up to the primary exhaust passage exit; hence, prospects for efficient turning of the exhaust flow are good. For $\delta_v = 45°$ (fig. 7(f)), a small separation bubble appears to form in the primary exhaust passage. This bubble appears to be very small, and therefore should have little effect on performance. At $\delta_v = 60°$ (fig. 7(g)), supersonic flow occurs over a large portion of the lower rotating flap in the primary exhaust passage. The fact that the pressures on the top surface of the lower rotating flap are considerably lower than on the bottom surface should help to provide a net normal force upward, which should improve resultant turning angle.

Performance Comparisons

Nozzle internal thrust ratio F/F_i, resultant thrust ratio F_r/F_i, discharge coefficient w_p/w_i, and resultant thrust-vector angle δ are presented in figure 8 as a function of NPR. Data are presented for each upper-rotating-flap configuration investigated at constant values of design thrust-vector angle δ_v. Faired lines with no symbols indicate resultant thrust ratio F_r/F_i. Also, the break in the F/F_i scale for $\delta_v = 45°$ (figs. 8(d) and (e)) allows the presentation of both resultant thrust ratio F_r/F_i and thrust ratio F/F_i on the same figure.

Effects of upper-rotating-flap configuration. As seen in figure 8, upper-rotating-flap configuration had very little effect on resultant thrust ratio F_r/F_i except at $\delta_v = 15°$. At $\delta_v = 15°$, the long upper rotating flap resulted in a 1-percent decrease in F_r/F_i when compared with the baseline and angled upper-rotating-flap configurations. The reason for this loss is not understood, but because the effects of upper-rotating-flap configuration on static-pressure distributions in the secondary passage are small, it is assumed that most of the loss takes place in the primary passage. Examination of the static pressure in the primary passage for the $\delta_v = 15°$ case (figs. 4 and 5) shows that static pressures on the top surface of the lower rotating flap remain higher for the long upper rotating flap than for either the baseline or angled upper rotating flaps. Also, it can be seen that the throat location on the lower rotating flap moves from $x''/l_{l,\mathrm{rot}} = 0.91$ for the long upper flap to approximately 0.82 for the baseline and angled upper flaps. This move causes more of the exhaust flow expansion to occur on the lower rotating flap for the baseline and angled upper flap than for the long upper flap.

In general, resultant thrust-vector angle varied with NPR. This variation is common for nozzles with an external expansion surface and is the result of the changing pressure distribution on the external expansion surfaces. The long upper rotating flap provided larger resultant thrust-vector angles than either the baseline or angled upper rotating flaps, probably because of the increased containment of exhaust flow on the upper surface of the lower rotating flap. Associated with these increases in resultant thrust-vector angle is an axial-thrust (body-axis) performance penalty. The reduced internal thrust ratio F/F_i of the long upper rotating flap is a result of a larger percentage of the thrust being turned away from the axial direction.

As might be expected, upper-rotating-flap configuration also affected nozzle discharge coefficient. In the unvectored-thrust mode ($\delta_v = 0°$), the baseline upper rotating flap provided the highest level of discharge coefficient, and the long upper rotating flap the lowest. Apparently, losses due to viscous effects, which result in a reduction in the amount of mass flow capable of being passed through the throat, increase with increased upper-flap and sidewall length. In fact, the increased length of the upper rotating flap causes a portion of the upper rotating flap to become an external expansion ramp. In this case, both the pressure distributions (table XII and fig. 7(c)) and resultant thrust-vector-angle data indicate that the throat plane may be skewed. This

is a common occurrence on single-expansion-ramp nozzles. (See refs. 19 and 22.) Skewing of the throat plane may reduce the efficiency with which the nozzle passes mass flow. It may also provide different values of effective throat area than the measured values. Once the nozzle was vectored ($\delta_v > 0°$), the long upper rotating flap produced the highest nozzle discharge coefficients, and the angled upper rotating flap produced the lowest discharge coefficients. One characteristic of both vectored and unvectored configurations is that nozzle discharge coefficient is not independent of NPR. Discharge coefficient tends to increase with increasing NPR, but the increases appear to be smaller at the higher vector angles. Unfortunately, little insight as to why this occurs could be gained from examination of the internal pressure distributions on the unvectored ($\delta_v = 0°$) configurations, because the nozzle throat was formed aft of the most downstream pressure orifice location. However, the pressure distributions for the vectored configurations suggest that throat location does vary with NPR in both the primary and secondary exhaust passages. In the primary exhaust passage, the static-pressure data indicate that throat location on the top surface of the lower rotating flap generally moves throughout the NPR range tested except when $\delta_v = 60°$, where the throat is upstream of the first pressure orifice location on the lower rotating flap. Throat location in the secondary exhaust passage (on the bottom surface of the lower rotating flap) appeared to vary only up to a nozzle pressure ratio of approximately 3.0. As would be expected from the above discussion, the largest amount of variation of nozzle discharge coefficient with NPR occurred between NPR = 2.0 and 3.0. (See fig. 8.)

Summary of design thrust-vector-angle effects. A summary of the effects of design thrust-vector angle on resultant thrust ratio and vector angle for configurations with the baseline upper rotating flap is shown in figure 9. All data are presented at a nominal nozzle pressure ratio of 3.0.

Except for the $\delta_v = 15°$ configuration, resultant thrust ratio levels remained high (within 1 percent of the unvectored nozzle) up to the maximum geometric vector angle tested. As discussed previously, the losses associated with the 15° vectoring configuration are believed to result from large overexpansion losses in the secondary exhaust passage. The relatively high levels of performance throughout the range of design vector angles investigated indicate that a majority of the exhaust flow turning is being accomplished with a subsonic exhaust flow where turning losses are small. This nozzle concept generally provided resultant thrust-vector angles equal to or greater than geometric (design) thrust-vector angles at NPR = 3.0. Also, the unvectored ($\delta_v = 0°$) nonaxisymmetric nozzle configurations investigated had peak static internal performance levels comparable with other unvectored convergent or low-expansion-ratio axisymmetric nozzles. (See refs. 26 to 29).

Conclusions

An investigation has been conducted at wind-off conditions in the static-test facility of the Langley 16-Foot Transonic Tunnel to determine the internal performance characteristics of a two-dimensional convergent nozzle with a thrust-vectoring capability up to 60°. Vectoring was accomplished by a downward rotation of a hinged upper convergent flap and a corresponding rotation of a center-pivoted lower convergent flap. The effects of geometric thrust-vector angle and upper-rotating-flap geometry on internal nozzle performance characteristics were investigated. Nozzle pressure ratio (NPR) was varied from 1.0 (jet off) to approximately 5.0. Results of this study indicate the following conclusions:

1. Unvectored two-dimensional convergent nozzles have peak static internal performance levels comparable with unvectored axisymmetric convergent nozzle levels.

2. The two-dimensional convergent nozzle concept investigated was, in general, highly effective in providing large thrust-vector angles (up to 60°) with little loss in resultant thrust ratio. The exception to this occurred at a design thrust-vector angle of 15°, where shock-induced separation in the secondary exhaust passage caused losses in resultant thrust ratio.

3. Upper-rotating-flap configuration had little effect on resultant thrust ratio except at a design thrust-vector angle of 15°, where the long upper rotating flap provided decreases in nozzle performance. The long upper rotating flap did, however, provide increased turning angles over baseline and angled flaps throughout the design thrust-vector angle and NPR range tested.

Langley Research Center
National Aeronautics and Space Administration
Hampton, VA 23665
November 1, 1984

References

1. Hiley, P. E.; Wallace, H. W.; and Booz, D. E.: Nonaxisymmetric Nozzles Installed in Advanced Fighter Aircraft. *J. Aircr.*, vol. 13, no. 12, Dec. 1976, pp. 1000–1006.
2. Capone, Francis J.: *Effects of Nozzle Exit Location and Shape on Propulsion-Induced Aerodynamic Characteristics Due to Vectoring Twin Nozzles at Mach Numbers From 0.40 to 1.2.* NASA TM X-3313, 1976.
3. Rolls, L. Stewart; and Aoyagi, Kiyoshi: Experimental Investigations of Thrust Vectoring Systems for VTOL Aircraft. AIAA Paper 77-805, July 1977.

4. Curry, Steven G.; Barnes, G. Ray; Jones, Thomas J.; and Hartill, William R.: Exhaust Nozzle Concepts for STOL Tactical Aircraft. AIAA-83-1226, June 1983.
5. Stevens, H. L.: *F-15/Nonaxisymmetric Nozzle System Integration Study Support Program.* NASA CR-135252, 1978.
6. Sedgwick, T. A.: Investigation of Non-Symmetric Two-Dimensional Nozzles Installed in Twin-Engine Tactical Aircraft. AIAA Paper No. 75-1319, Sept.–Oct. 1975.
7. *F-15 2-D Nozzle System Integration Study. Volume I—Technical Report.* NASA CR-145295, 1978.
8. Bergman, D.; Mace, J. L.; and Thayer, E. B.: Non-Axisymmetric Nozzle Concepts for an F-111 Test Bed. AIAA Paper No. 77-841, July 1977.
9. Schnell, W. C.; Grossman, R. L.; and Hoff, G. E.: Comparison of Non-Axisymmetric and Axisymmetric Nozzles Installed on a V/STOL Fighter Model. [Preprint] 770983, Soc. Automot. Eng., Nov. 1977.
10. Schnell, W. C.; and Grossman, R. L.: Vectoring Non-Axisymmetric Nozzle Jet Induced Effects on a V/STOL Fighter Model. AIAA Paper 78-1080, July 1978.
11. Hiley, P. E.; and Bowers, D. L.: Advanced Nozzle Integration for Supersonic Strike Fighter Application. AIAA-81-1441, July 1981.
12. Capone, Francis J.; Hunt, Brian L.; and Poth, Greg E.: Subsonic/Supersonic Unvectored Aeropropulsive Characteristics of Nonaxisymmetric Nozzles Installed on an F-18 Model. AIAA-81-1445, July 1981.
13. Berrier, Bobby L.; Palcza, J. Lawrence; and Richey, G. Keith: Nonaxisymmetric Nozzle Technology Program An Overview. AIAA Paper 77-1225, Aug. 1977.
14. Capone, Francis J.; and Berrier, Bobby L.: *Investigation of Axisymmetric and Nonaxisymmetric Nozzles Installed on a 0.10-Scale F-18 Prototype Airplane Model.* NASA TP-1638, 1980.
15. Capone, Francis J.: *Aeropropulsive Characteristics at Mach Numbers up to 2.2 of Axisymmetric and Nonaxisymmetric Nozzles Installed on an F-18 Model.* NASA TP-2044, 1982.
16. Capone, Francis J.; and Reubush, David E.: *Effects of Varying Podded Nacelle-Nozzle Installations on Transonic Aeropropulsive Characteristics of a Supersonic Fighter Aircraft.* NASA TP-2120, 1983.
17. Mason, Mary L.; and Capone, Francis J.: *Aeropropulsive Characteristics of Twin Single-Expansion-Ramp Vectoring Nozzles Installed With Forward-Swept Wings and Canards.* NASA TP-2133, 1983.
18. Lander, J. A.; Nash, D. O.; and Palcza, J. Lawrence: Augmented Deflector Exhaust Nozzle (ADEN) Design for Future Fighters. AIAA Paper No. 75-1318, Sept.–Oct. 1975.
19. Berrier, Bobby L.; and Re, Richard J.: *Effect of Several Geometric Parameters on the Static Internal Performance of Three Nonaxisymmetric Nozzle Concepts.* NASA TP-1468, 1979.
20. Re, Richard J.; and Berrier, Bobby L.: *Static Internal Performance of Single Expansion-Ramp Nozzles With Thrust Vectoring and Reversing.* NASA TP-1962, 1982.
21. Capone, Francis J.: *Static Performance of Five Twin-Engine Nonaxisymmetric Nozzles With Vectoring and Reversing Capability.* NASA TP-1224, 1978.
22. Berrier, Bobby L.; and Leavitt, Laurence D.: *Static Internal Performance of Single-Expansion-Ramp Nozzles With Thrust-Vectoring Capability up to 60°.* NASA TP-2364, 1984.
23. Berrier, B. L.; and Re, R. J.: A Review of Thrust-Vectoring Schemes for Fighter Aircraft. AIAA Paper No. 78-1023, July 1978.
24. Re, Richard J.; and Leavitt, Laurence D.: *Static Internal Performance Including Thrust Vectoring and Reversing of Two-Dimensional Convergent-Divergent Nozzles.* NASA TP-2253, 1984.
25. Straight, David M.; and Cullom, Richard R.: Performance of a 2D-CD Nonaxisymmetric Exhaust Nozzle on a Turbojet Engine of Altitude. AIAA-82-1137, June 1982.
26. Reubush, David E.; and Mercer, Charles E.: *Exhaust-Nozzle Characteristics for a Twin-Jet Variable-Wing-Sweep Fighter Airplane Model at Mach Numbers to 2.2.* NASA TM X-2947, 1974.
27. Lee, Edwin E., Jr.; and Runckel, Jack F.: *Performance of Closely Spaced Twin-Jet Afterbodies With Different Inboard-Outboard Fairing and Nozzle Shapes.* NASA TM X-2329, 1971.
28. Reubush, David E.; and Runckel, Jack F.: *Effect of Fineness Ratio on Boattail Drag of Circular-Arc Afterbodies Having Closure Ratios of 0.50 With Jet Exhaust at Mach Numbers up to 1.30.* NASA TN D-7192, 1973.
29. Mercer, Charles E.; and Berrier, Bobby L.: *Effect of Afterbody Shape, Nozzle Type, and Engine Lateral Spacing on the Installed Performance of a Twin-Jet Afterbody Model.* NASA TM X-1855, 1969.

TABLE I. IMPORTANT CONFIGURATION PARAMETERS

Conf	δ_v, deg	δ_l, deg	δ_u, deg	Upper flap	Sidewall	*h_u, in.	*h_l, in.	*A_t, in^2
1	0	−12.7	6.9	Baseline	Baseline			7.914
2	15	15.0	44.3	↓	↓	1.593	0.384	7.904
3	30	30.0	56.4	↓	↓	1.355	.682	8.144
4	45	45.0	60.6	↓	↓	1.162	.936	8.390
5	60	60.0	51.9	↓	↓	1.130	1.072	8.806
6	0	−12.7	15.0	Angled	↓			7.914
7	15	15.0	52.4	↓	↓	1.159	.384	7.896
8	30	30.0	64.5	↓	↓	1.350	.680	8.116
9	45	45.0	68.7	↓	↓	1.162	.936	8.388
10	60	60.0	60.0	↓	↓	1.190	1.072	9.046
11	0	−12.7	6.9	Long	Extended			7.834
12	15	15.0	44.3	↓	↓	1.395	.381	7.102
13	30	30.0	56.4	↓	↓	1.153	.682	7.338
14	45	45.0	60.6	↓	↓	1.032	.936	7.870
15	60	60.0	51.9	↓	↓	1.125	1.072	8.786

*Measured values.

TABLE II. RATIO OF INTERNAL STATIC PRESSURE TO JET TOTAL PRESSURE FOR CONFIGURATION 1

(a) Flap pressures

Upper flap pressures

NPR	$x'/l_{u,rot}$							
	-1.396	-.823	-.537	-.251	.178	.392	.606	.819
2.003	.8595	.8693	.8903	.8707	.7279	.7195	.6895	.6448
2.524	.8590	.8685	.8932	.8698	.7253	.7166	.6861	.6407
3.012	.8597	.8689	.8965	.8700	.7258	.7170	.6868	.6405
3.978	.8603	.8690	.9005	.8708	.7270	.7181	.6882	.6413
5.020	.8599	.8674	.9025	.8704	.7278	.7187	.6896	.6416

Fixed lower flap pressures

NPR	$x'/l_{l,fixed}$		
	.385	.605	.846
2.003	.8526	.8503	.8810
2.524	.8516	.8490	.8800
3.012	.8522	.8491	.8807
3.978	.8524	.8488	.8810
5.020	.8515	.8474	.8802

Lower rotating flap pressures

Top

NPR	$x''/l_{l,rot}$							
	.131	.242	.353	.463	.574	.685	.796	.906
2.003	.8624	.8332	.8066	.7638	.7418	.7230	.6987	.6358
2.524	.8624	.8315	.8050	.7621	.7389	.7211	.6961	.6326
3.012	.8634	.8320	.8051	.7622	.7382	.7209	.6958	.6325
3.978	.8641	.8329	.8052	.7615	.7371	.7205	.6951	.6327
5.020	.8627	.8330	.8039	.7597	.7362	.7195	.6940	.6315

TABLE II. Concluded

(b) Sidewall pressures

NPR	PRSID1	PRSID2	PRSID3	PRSID4	PRSID5	PRSID6	PRSID7	PRSID8	PRSID9	PRSID10
2.003	.8511	.8425	.8589	.8490	.8365	.8591	.8522	.8313	.8662	.8580
2.524	.8498	.8416	.8571	.8481	.8356	.8577	.8514	.8306	.8642	.8565
3.012	.8502	.8419	.8565	.8484	.8360	.8581	.8517	.8305	.8650	.8573
3.978	.8504	.8422	.8554	.8479	.8363	.8563	.8515	.8299	.8642	.8567
5.020	.8497	.8412	.8533	.8469	.8356	.8575	.8503	.8287	.8633	.8555

NPR	PRSID11	PRSID12	PRSID17	PRSID18	PRSID19	PRSID20	PRSID21	PRSID22	PRSID23	PRSID24
2.003	.8422	.8243	.8283	.8108	.7558	.8081	.7643	.7868	.7666	.7492
2.524	.8408	.8228	.8276	.8096	.7541	.8072	.7626	.7850	.7638	.7467
3.012	.8414	.8230	.8277	.8095	.7544	.8074	.7625	.7854	.7642	.7467
3.978	.8407	.8223	.8274	.8090	.7546	.8072	.7625	.7857	.7651	.7470
5.020	.8394	.8208	.8260	.8075	.7543	.8061	.7617	.7855	.7659	.7464

NPR	PRSID25	PRSID26	PRSID27	PRSID28	PRSID29	PRSID30	PRSID31	PRSID33	PRSID36
2.003	.7294	.6978	.7677	.7268	.6731	.7472	.5867	.5906	.5822
2.524	.7273	.6950	.7661	.7279	.6699	.7457	.5797	.5827	.5746
3.012	.7274	.6954	.7663	.7261	.6699	.7458	.5802	.5836	.5743
3.978	.7275	.6956	.7666	.7265	.6700	.7460	.5807	.5834	.5744
5.020	.7269	.6951	.7660	.7275	.6699	.7457	.5806	.5830	.5744

TABLE III. RATIO OF INTERNAL STATIC PRESSURE TO JET TOTAL PRESSURE FOR CONFIGURATION 2

(a) Flap pressures

Upper flap pressures

NPR	$x'/l_{u,rot}$							
	-1.396	-.823	-.537	-.251	.178	.392	.606	.819
1.991	.8856	.9130	.9375	.9360	.9186	.8812	.8324	.7651
2.508	.8850	.9097	.9388	.9339	.9154	.8762	.8251	.7549
3.000	.8844	.9090	.9412	.9339	.9150	.8756	.8240	.7516
2.983	.8845	.9090	.9411	.9339	.9151	.8754	.8240	.7517
3.996	.8841	.9082	.9450	.9349	.9158	.8762	.8251	.7513
5.020	.8836	.9069	.9467	.9355	.9162	.8765	.8270	.7516

Fixed lower flap pressures

NPR	$x'/l_{l,fixed}$			
	.385	.605	.846	.969
1.991	.8305	.7676	.3585	.4830
2.508	.8272	.7632	.3402	.3782
3.000	.8265	.7620	.3405	.3267
2.983	.8265	.7618	.3405	.3228
3.996	.8264	.7611	.3408	.2650
5.020	.8261	.7602	.3400	.1620

Lower rotating flap pressures

Top

NPR	$x''/l_{l,rot}$							
	.131	.242	.353	.463	.574	.685	.796	.906
1.991	.7702	.7784	.7579	.6994	.6657	.6330	.5998	.5442
2.508	.7609	.7681	.7466	.6827	.6411	.5996	.5534	.4803
3.000	.7586	.7654	.7435	.6777	.6329	.5879	.5366	.4572
2.983	.7586	.7654	.7434	.6778	.6330	.5880	.5370	.4579
3.996	.7569	.7646	.7419	.6754	.6290	.5830	.5267	.4378
5.020	.7554	.7641	.7406	.6736	.6274	.5814	.5251	.4364

Bottom

NPR	$x''/l_{l,rot}$							
	.131	.242	.353	.463	.574	.685	.796	.906
1.991	.2977	.4003	.5197	.4999	.5009	.5123	.5115	.5216
2.508	.1785	.2677	.3707	.4356	.4102	.4108	.4067	.4085
3.000	.1783	.1252	.2303	.3061	.3786	.3537	.3712	.3231
2.983	.1781	.1253	.2323	.3128	.3846	.3502	.3729	.3211
3.996	.1784	.1268	.1357	.1867	.1949	.2163	.2457	.2732
5.020	.1793	.1276	.0874	.1609	.1643	.1655	.1691	.1789

TABLE III. Concluded

(b) Sidewall pressures

NPR	PRSID1	PPSID2	PRSID3	PRSID4	PRSID5	PRSID6	PRSID7	PRSID8	PRSID9	PRSID10	PRSID12
1.991	.8693	.8619	.8538	.8559	.8386	.8280	.8496	.7925	.4263	.2157	.7841
2.508	.8647	.8567	.8660	.8512	.8317	.8250	.8432	.7835	.4236	.2100	.7751
3.000	.8632	.8553	.8619	.8497	.8301	.8236	.8414	.7808	.4222	.2100	.7726
2.983	.8633	.8553	.8658	.8496	.8299	.8239	.8414	.7808	.4226	.2098	.7726
3.996	.8626	.8543	.8628	.8485	.8291	.8226	.8404	.7792	.4205	.2072	.7714
5.020	.8620	.8536	.8563	.8472	.8283	.8218	.8394	.7778	.4203	.2063	.7700

NPR	PRSID13	PRSID14	PRSID15	PRSID17	PRSID18	PRSID19	PRSID20	PRSID21	PRSID22	PRSID23
1.991	.4850	.4759	.4985	.9227	.8855	.8838	.8457	.8348	.7966	.7851
2.508	.3563	.3072	.3451	.9210	.8819	.8794	.8400	.8285	.7878	.7752
3.000	.2712	.2106	.2457	.9197	.8806	.8782	.8378	.8265	.7853	.7728
2.983	.2732	.2112	.2471	.9194	.8805	.8781	.8378	.8264	.7853	.7723
3.996	.2106	.1108	.1192	.9180	.8794	.8773	.8364	.8251	.7844	.7725
5.020	.1932	.1051	.1165	.9171	.8782	.8773	.8353	.8248	.7840	.7736

NPR	PRSID24	PRSID25	PRSID26	PRSID27	PRSID28	PRSID29	PRSID30	PRSID31	PRSID33	PRSID36
1.991	.7734	.7470	.6902	.7451	.6983	.5948	.6578	.5013	.5132	.5299
2.508	.7624	.7341	.6723	.7326	.6765	.5345	.6350	.3979	.4167	.4442
3.000	.7596	.7307	.6695	.7292	.6704	.4927	.6288	.3325	.3583	.4034
2.983	.7596	.7307	.6694	.7292	.6698	.4939	.6288	.3345	.3599	.4046
3.996	.7584	.7292	.6682	.7281	.6692	.4691	.6266	.2495	.2789	.3487
5.020	.7579	.7288	.6678	.7275	.6774	.4687	.6255	.1984	.2359	.3228

TABLE IV. RATIO OF INTERNAL STATIC PRESSURE TO JET TOTAL PRESSURE FOR CONFIGURATION 3

(a) Flap pressures

Upper flap pressures

NPR	$x'/l_{u,rot}$							
	-1.396	-.823	-.537	-.251	.178	.392	.606	.819
2.009	.8882	.9192	.9417	.9411	.9377	.9033	.8519	.7797
2.511	.8856	.9159	.9434	.9395	.9360	.9004	.8471	.7711
3.006	.8861	.9162	.9469	.9406	.9368	.9007	.8470	.7697
4.019	.8863	.9165	.9519	.9427	.9384	.9020	.8487	.7695
5.028	.8853	.9145	.9531	.9431	.9386	.9019	.8496	.7686

Fixed lower flap pressures

NPR	$x'/l_{l,fixed}$			
	.385	.605	.846	.969
2.009	.7958	.7001	.4291	.4865
2.511	.7933	.6965	.2679	.3788
3.006	.7934	.6958	.2376	.3034
4.019	.7938	.6951	.2371	.1850
5.028	.7930	.6936	.2361	.1423

Lower rotating flap pressures

Top

NPR	$x''/l_{l,rot}$							
	.131	.242	.353	.463	.574	.685	.796	.906
2.009	.6947	.7282	.6901	.5956	.5374	.5147	.5050	.5234
2.511	.6826	.7170	.6774	.5786	.4938	.4433	.4039	.3487
3.006	.6849	.7143	.6745	.5757	.4755	.4214	.3725	.3071
4.019	.6893	.7134	.6736	.5754	.4683	.4060	.3440	.2704
5.028	.6892	.7121	.6721	.5744	.4673	.4059	.3429	.2656

Bottom

NPR	$x''/l_{l,rot}$							
	.131	.242	.353	.463	.574	.685	.796	.906
2.009	.4896	.5246	.5295	.4721	.3669	.5423	.5240	.5220
2.511	.4882	.3622	.2563	.3382	.2884	.4294	.4982	.4272
3.006	.4889	.3630	.2545	.1685	.1934	.2676	.3119	.3581
4.019	.4923	.3646	.2551	.1694	.0924	.1769	.1728	.1788
5.028	.4949	.3652	.2554	.1696	.0922	.0709	.0572	.1103

TABLE IV. Concluded

(b) Sidewall pressures

NPR	PRSID1	PRSID2	PRSID3	PRSID4	PRSID5	PRSID6	PRSID7	PRSID9	PRSID10	PRSID11
2.009	.8639	.8546	.8289	.8705	.8002	.7551	.8843	.4579	.3845	.3972
2.511	.8605	.8500	.8273	.8686	.7929	.7529	.8836	.4509	.3793	.3910
3.006	.8601	.8492	.8281	.8683	.7915	.7524	.8842	.4504	.3791	.3903
4.019	.8600	.8483	.8280	.8681	.7901	.7519	.8851	.4494	.3795	.3896
5.028	.8588	.8465	.8264	.8667	.7879	.7507	.8850	.4483	.3811	.3895

NPR	PRSID13	PRSID14	PRSID15	PRSID16	PRSID17	PRSID18	PRSID19	PRSID20	PRSID21	PRSID22
2.009	.4907	.4920	.5220	.5263	.9347	.8896	.9233	.8301	.8301	.7581
2.511	.3758	.3478	.2757	.2491	.9332	.8868	.9193	.8239	.8240	.7480
3.006	.2963	.2296	.2459	.2470	.9329	.8863	.9187	.8228	.8232	.7460
4.019	.1716	.2143	.2460	.2493	.9314	.8849	.9164	.8215	.8230	.7455
5.028	.1408	.2137	.2466	.2477	.9291	.8829	.9137	.8193	.8213	.7443

NPR	PRSID23	PRSID24	PRSID25	PRSID27	PRSID28	PRSID29	PRSID30	PRSID31	PRSID33	PRSID36
2.009	.7472	.7262	.6982	.6897	.6130	.5176	.5644	.4971	.4968	.5119
2.511	.7359	.7136	.6833	.6752	.5752	.4260	.5288	.3978	.3972	.4080
3.006	.7339	.7110	.6820	.6716	.5569	.3676	.5207	.3320	.3318	.3447
4.019	.7344	.7112	.6824	.6711	.5560	.2951	.5188	.2483	.2481	.2725
5.028	.7347	.7107	.6826	.6702	.5533	.2524	.5191	.1984	.1984	.2316

TABLE V. RATIO OF INTERNAL STATIC PRESSURE TO JET TOTAL PRESSURE FOR CONFIGURATION 4

(a) Flap pressures

Upper flap pressures

	$x'/l_{u,rot}$							
NPR	-1.396	-.823	-.537	-.251	.178	.392	.606	.819
2.015	.8850	.9166	.9396	.9399	.9396	.9000	.8363	.7504
2.507	.8833	.9150	.9418	.9383	.9379	.8991	.8338	.7435
3.038	.8837	.9153	.9451	.9389	.9381	.9001	.8348	.7435
3.987	.8843	.9154	.9497	.9406	.9400	.9012	.8364	.7436
5.040	.8843	.9146	.9520	.9419	.9417	.9024	.8388	.7446

Fixed lower flap pressures

	$x'/l_{l,fixed}$			
NPR	.385	.605	.846	.969
2.015	.7820	.6813	.3853	.4733
2.507	.7786	.6763	.2537	.3691
3.038	.7787	.6756	.2209	.2667
3.987	.7795	.6752	.2217	.1959
5.040	.7794	.6744	.2211	.1936

Lower rotating flap pressures

Top

	$x''/l_{l,rot}$							
NPR	.131	.242	.353	.463	.574	.685	.796	.906
2.015	.4566	.6114	.6007	.5173	.4060	.4466	.5410	.5362
2.507	.4331	.5954	.5722	.4853	.3397	.3239	.3138	.3464
3.038	.4331	.5981	.5642	.4700	.3026	.2685	.2528	.2212
3.987	.4389	.6017	.5612	.4679	.2970	.2423	.2057	.1626
5.040	.4496	.6038	.5596	.4673	.2968	.2413	.2029	.1531

Bottom

	$x''/l_{l,rot}$							
NPR	.131	.242	.353	.463	.574	.685	.796	.906
1.000	.9851	1.0004	1.0002	.9993	.9997	.9997	.9999	.9998
2.015	.7160	.6285	.5584	.4803	.3589	.4224	.5546	.5358
2.507	.7024	.5903	.4732	.3811	.2834	.2633	.3187	.4410
3.038	.7042	.5897	.4632	.3322	.1950	.1956	.2753	.2890
3.987	.7136	.5906	.4646	.3328	.1951	.1521	.1209	.0964
5.040	.7128	.5911	.4654	.3326	.1955	.1522	.1211	.0971

TABLE V. Concluded

(b) Sidewall pressures

NPR	PRSID1	PRSID2	PRSID3	PRSID4	PRSID5	PRSID6	PRSID7	PRSID9	PRSID10	PRSID11
2.015	.8605	.8615	.8106	.8484	.8529	.7320	.8163	.5048	.5821	.6068
2.507	.8569	.8584	.8090	.8447	.8497	.7266	.8114	.4723	.5409	.5671
3.038	.8570	.8582	.8082	.8446	.8489	.7262	.8115	.4703	.5404	.5664
3.987	.8573	.8584	.8095	.8446	.8485	.7266	.8116	.4688	.5398	.5663
5.040	.8574	.8581	.8094	.8446	.8480	.7265	.8115	.4680	.5389	.5662

NPR	PRSID13	PRSID14	PRSID15	PRSID16	PRSID17	PRSID18	PRSID19	PRSID20	PRSID21	PRSID22
2.015	.4601	.4948	.5232	.5328	.9330	.8743	.9217	.7657	.8011	.6329
2.507	.3747	.4202	.4354	.4347	.9319	.8722	.9200	.7587	.7962	.6177
3.038	.2544	.3202	.3935	.4207	.9314	.8713	.9188	.7580	.7963	.6184
3.987	.2029	.3159	.3937	.4210	.9306	.8703	.9177	.7573	.7967	.6210
5.040	.1968	.3128	.3936	.4200	.9297	.8694	.9169	.7565	.7969	.6241

NPR	PRSID23	PRSID24	PRSID25	PRSID27	PRSID28	PRSID29	PRSID30	PRSID31	PRSID33	PRSID36
2.015	.6476	.6545	.6066	.5970	.5469	.4953	.5211	.4952	.4955	.4941
2.507	.6331	.6404	.5882	.5650	.4690	.3980	.4805	.3978	.3982	.3987
3.038	.6316	.6401	.5869	.5597	.4216	.3297	.4555	.3283	.3284	.3322
3.987	.6331	.6409	.5869	.5596	.3974	.2556	.4488	.2500	.2501	.2612
5.040	.6359	.6421	.5871	.5603	.3960	.2064	.4480	.1977	.1978	.2102

TABLE VI. RATIO OF INTERNAL STATIC PRESSURE TO JET TOTAL PRESSURE FOR CONFIGURATION 5

(a) Flap pressures

Upper flap pressures

	$x'/l_{u,rot}$							
NPR	-1.396	-.823	-.537	-.251	.178	.392	.606	.819
2.025	.8747	.9031	.9279	.9282	.9099	.8496	.7594	.6548
2.496	.8713	.9001	.9287	.9264	.9065	.8406	.7411	.6232
2.998	.8719	.9003	.9321	.9269	.9069	.8406	.7410	.6226
3.356	.8721	.9001	.9338	.9274	.9073	.8407	.7411	.6224

Fixed lower flap pressures

	$x'/l_{l,fixed}$			
NPR	.385	.605	.846	.969
2.025	.7776	.6782	.2987	.4581
2.496	.7714	.6703	.2307	.3437
2.998	.7714	.6692	.2304	.2782
3.356	.7715	.6689	.2301	.2718

Lower rotating flap pressures

Top

	$x''/l_{l,rot}$							
NPR	.131	.242	.353	.463	.574	.685	.796	.906
2.025	.3218	.3236	.3527	.3979	.4315	.4598	.4829	.5003
2.496	.0660	.2027	.3056	.3241	.3291	.4100	.4581	.4472
2.998	.0654	.2013	.3046	.3246	.2120	.1743	.3078	.3274
3.356	.0654	.2010	.3044	.3252	.2128	.1740	.1502	.2467

Bottom

	$x''/l_{l,rot}$							
NPR	.131	.242	.353	.463	.574	.685	.796	.906
2.025	.8773	.7893	.6957	.5590	.4256	.4181	.5524	.5176
2.496	.8715	.7741	.6651	.5125	.3390	.3541	.3097	.4048
2.998	.8719	.7740	.6664	.5116	.3260	.2689	.2639	.2458
3.356	.8721	.7741	.6671	.5119	.3262	.2669	.2363	.2220

TABLE VI. Concluded

(b) Sidewall pressures

NPR	PRSID1	PRSID2	PRSID3	PRSID4	PRSID5	PRSID6	PRSID7	PRSID8	PRSID9	PRSID10	PRSID11
2.025	.8560	.8777	.8072	.8420	.9052	.7303	.8196	.8482	.5383	.6561	.7132
2.496	.8506	.8737	.8017	.8363	.9008	.7219	.8126	.8370	.5102	.6258	.6869
2.998	.8511	.8737	.8020	.8358	.9014	.7217	.8122	.8369	.5079	.6258	.6861
3.356	.8513	.8743	.8017	.8360	.9017	.7218	.8120	.8368	.5067	.6254	.6860

NPR	PRSID12	PRSID13	PRSID14	PRSID15	PRSID16	PRSID17	PRSID18	PRSID19	PRSID20	PRSID21	PRSID22
2.025	.7636	.4613	.5395	.5959	.6242	.9116	.8379	.8570	.6195	.7066	.3631
2.496	.7412	.3708	.4340	.5333	.5770	.9078	.8301	.8488	.5889	.6829	.1783
2.998	.7407	.2972	.4241	.5297	.5754	.9071	.8299	.8483	.5884	.6826	.1769
3.356	.7404	.2866	.4216	.5294	.5743	.9067	.8299	.8481	.5880	.6825	.1761

NPR	PRSID23	PRSID24	PRSID25	PRSID26	PRSID27	PRSID28	PRSID29	PRSID30	PRSID31	PRSID33	PRSID36
2.025	.4820	.5432	.5684	.4918	.3525	.3824	.5024	.4207	.4928	.4925	.4962
2.496	.3751	.4809	.5248	.3999	.2531	.2861	.3991	.3650	.3998	.3995	.4042
2.998	.3726	.4806	.5245	.3409	.1998	.2882	.3225	.3184	.3327	.3323	.3429
3.356	.3717	.4805	.5244	.3137	.1999	.2881	.2854	.3115	.2975	.2971	.3080

TABLE VII. RATIO OF INTERNAL STATIC PRESSURE TO JET TOTAL PRESSURE FOR CONFIGURATION 6

(a) Flap pressures

Upper flap pressures

NPR	$x'/l_{u,rot}$							
	-1.396	-.823	-.537	-.251	.178	.392	.606	.819
2.012	.8614	.8701	.8904	.8687	.7462	.7805	.7972	.7249
2.500	.8595	.8682	.8923	.8663	.7415	.7766	.7943	.7194
3.006	.8596	.8680	.8950	.8665	.7405	.7765	.7953	.7194
4.048	.8604	.8680	.8999	.8670	.7408	.7776	.7988	.7207
5.005	.8596	.8665	.9014	.8666	.7403	.7781	.8015	.7212

Fixed lower flap pressures

NPR	$x'/l_{l,fixed}$		
	.385	.605	.846
2.012	.8552	.8537	.8828
2.500	.8529	.8509	.8811
3.006	.8527	.8503	.8813
4.048	.8536	.8499	.8818
5.005	.8523	.8486	.8810

Lower rotating flap pressures

Top

NPR	$x''/l_{l,rot}$							
	.131	.242	.353	.463	.574	.685	.796	.906
2.012	.8651	.8370	.8122	.7722	.7530	.7360	.7129	.6501
2.500	.8639	.8341	.8091	.7687	.7481	.7316	.7077	.6441
3.006	.8641	.8339	.8085	.7680	.7456	.7306	.7066	.6431
4.048	.8648	.8349	.8083	.7670	.7450	.7300	.7060	.6424
5.005	.8636	.8349	.8072	.7651	.7441	.7296	.7049	.6421

TABLE VII. Concluded

(b) Sidewall pressures

NPR	PRSID1	PRSID2	PRSID3	PRSID4	PRSID5	PRSID6	PRSID7	PRSID8	PRSID9	PRSID10
2.012	.8540	.8451	.8553	.8522	.8397	.8598	.8546	.8354	.8703	.8609
2.500	.8513	.8424	.8541	.8494	.8373	.8574	.8525	.8330	.8660	.8587
3.006	.8508	.8419	.8526	.8488	.8370	.8573	.8522	.8322	.8681	.8594
4.048	.8510	.8422	.8540	.8487	.8372	.8577	.8521	.8319	.8692	.8602
5.005	.8504	.8414	.8529	.8477	.8368	.8572	.8510	.8308	.8689	.8596

NPR	PRSID11	PRSID12	PRSID17	PRSID18	PRSID19	PRSID20	PRSID21	PRSID22	PRSID23	PRSID24
2.012	.8437	.8272	.8309	.8139	.7585	.8135	.7757	.7941	.7760	.7625
2.500	.8415	.8248	.8284	.8110	.7545	.8107	.7721	.7904	.7718	.7583
3.006	.8415	.8246	.8281	.8105	.7546	.8105	.7717	.7897	.7713	.7576
4.048	.8417	.8245	.8276	.8096	.7552	.8101	.7713	.7899	.7725	.7576
5.005	.8407	.8234	.8262	.8081	.7547	.8088	.7704	.7895	.7730	.7568

NPR	PRSID25	PRSID26	PRSID27	PRSID28	PRSID29	PRSID30	PRSID31	PRSID33	PRSID36
2.012	.7481	.7321	.7768	.7316	.6914	.7572	.6028	.5986	.6041
2.500	.7437	.7283	.7731	.7322	.6856	.7522	.5930	.5884	.5968
3.006	.7434	.7276	.7727	.7320	.6851	.7510	.5929	.5878	.5976
4.048	.7433	.7287	.7729	.7331	.6851	.7506	.5943	.5877	.5982
5.005	.7427	.7281	.7722	.7335	.6849	.7499	.5956	.5876	.5984

TABLE VIII. RATIO OF INTERNAL STATIC PRESSURE TO JET TOTAL PRESSURE FOR CONFIGURATION 7

(a) Flap pressures

Upper flap pressures

NPR	$x'/l_{u,rot}$							
	-1.396	-.823	-.537	-.251	.178	.392	.606	.819
2.001	.8913	.9161	.9400	.9375	.9228	.9028	.8881	.8178
2.507	.8868	.9104	.9391	.9332	.9191	.8965	.8814	.8070
3.050	.8855	.9089	.9412	.9326	.9175	.8953	.8805	.8045
4.038	.8849	.9079	.9449	.9332	.9186	.8961	.8829	.8046
5.040	.8846	.9065	.9462	.9336	.9192	.8969	.8861	.8049

Fixed lower flap pressures

NPR	$x'/l_{l,fixed}$			
	.385	.605	.846	.969
2.001	.8351	.7743	.3790	.4855
2.507	.8291	.7675	.3415	.3743
3.050	.8280	.7655	.3411	.3014
4.038	.8278	.7646	.3413	.1499
5.040	.8278	.7637	.3411	.1406

Lower rotating flap pressures

Top

NPR	$x''/l_{l,rot}$							
	.131	.242	.353	.463	.574	.685	.796	.906
2.001	.7839	.7922	.7737	.7190	.6845	.6506	.6133	.5535
2.507	.7712	.7786	.7593	.6992	.6576	.6151	.5672	.4924
3.050	.7672	.7747	.7546	.6922	.6476	.6019	.5491	.4675
4.038	.7652	.7733	.7523	.6885	.6411	.5929	.5347	.4459
5.040	.7636	.7733	.7515	.6869	.6398	.5918	.5332	.4428

Bottom

NPR	$x''/l_{l,rot}$							
	.131	.242	.353	.463	.574	.685	.796	.906
2.001	.3423	.3938	.5145	.5005	.4988	.5100	.5087	.5191
2.507	.1796	.2897	.3393	.4404	.4082	.4093	.4055	.4094
3.050	.1803	.1252	.2180	.2804	.3682	.3734	.3504	.3439
4.038	.1817	.1266	.1485	.1876	.1921	.2052	.2267	.2506
5.040	.1818	.1275	.0677	.1565	.1608	.1632	.1660	.1694

TABLE VIII. Concluded

(b) Sidewall pressures

NPR	PRSID1	PRSID2	PRSID3	PRSID4	PRSID5	PRSID6	PRSID7	PRSID8	PRSID9	PRSID10	PRSID12
2.001	.8747	.8694	.8663	.8633	.8491	.8294	.8603	.8072	.4295	.2241	.7993
2.517	.8672	.8610	.8521	.8548	.8394	.8226	.8502	.7966	.4275	.2086	.7864
3.050	.8650	.8597	.8502	.8520	.8364	.8213	.8467	.7913	.4273	.2088	.7823
4.038	.8642	.8574	.8528	.8506	.8347	.8217	.8444	.7887	.4278	.2085	.7804
5.040	.8639	.8568	.8519	.8497	.8344	.8216	.8433	.7873	.4279	.2078	.7792

NPR	PRSID13	PRSID14	PRSID15	PRSID17	PRSID18	PRSID19	PRSID20	PRSID21	PRSID22	PRSID23
2.001	.4850	.4926	.4940	.9261	.8933	.9031	.8578	.8566	.8127	.8027
2.517	.3593	.2695	.3317	.9219	.8869	.8974	.8493	.8486	.8007	.7914
3.050	.2603	.1285	.1126	.9206	.8852	.8959	.8465	.8462	.7969	.7879
4.038	.1448	.0998	.1061	.9185	.8842	.8950	.8446	.8447	.7954	.7871
5.040	.1024	.0981	.1056	.9175	.8833	.8943	.8436	.8443	.7954	.7882

NPR	PRSID24	PRSID25	PRSID26	PRSID27	PRSID28	PRSID29	PRSID30	PRSID31	PRSID33	PRSID36
2.001	.7952	.7746	.7127	.7630	.7189	.6052	.6766	.5001	.5092	.5405
2.517	.7820	.7594	.6924	.7472	.6948	.5453	.6513	.3989	.4072	.4576
3.050	.7778	.7543	.6878	.7423	.6857	.5098	.6427	.3276	.3375	.4113
4.038	.7750	.7518	.6896	.7403	.6807	.4721	.6389	.2471	.2672	.3631
5.040	.7758	.7516	.6900	.7398	.6800	.4671	.6384	.1979	.2236	.3368

TABLE IX. RATIO OF INTERNAL STATIC PRESSURE TO JET TOTAL PRESSURE FOR CONFIGURATION 8

(a) Flap pressures

Upper flap pressures

	$x'/l_{u,rot}$							
NPR	-1.396	-.823	-.537	-.251	.178	.392	.606	.819
2.015	.8922	.9208	.9445	.9429	.9403	.9193	.8996	.8300
2.508	.8887	.9180	.9455	.9408	.9388	.9160	.8963	.8226
2.989	.8880	.9173	.9479	.9408	.9388	.9155	.8959	.8206
4.047	.8880	.9169	.9530	.9426	.9407	.9172	.8989	.8207
4.999	.8875	.9156	.9544	.9434	.9414	.9181	.9021	.8211

Fixed lower flap pressures

	$x'/l_{l,fixed}$			
NPR	.385	.605	.846	.969
2.015	.7998	.7046	.4233	.4853
2.508	.7964	.6999	.2729	.3782
2.989	.7957	.6994	.2401	.3023
4.047	.7959	.6974	.2395	.1595
4.999	.7956	.6965	.2386	.1430

Lower rotating flap pressures

Top

	$x''/l_{l,rot}$							
NPR	.131	.242	.353	.463	.574	.685	.796	.906
2.015	.7347	.7467	.7096	.6169	.5567	.5263	.5067	.5169
2.508	.7211	.7340	.6947	.5936	.5127	.4596	.4161	.3578
2.989	.7178	.7298	.6897	.5877	.4957	.4356	.3828	.3141
4.047	.7181	.7276	.6869	.5852	.4795	.4120	.3528	.2819
4.999	.7185	.7273	.6860	.5845	.4778	.4095	.3442	.2670

Bottom

	$x''/l_{l,rot}$							
NPR	.131	.242	.353	.463	.574	.685	.796	.906
2.015	.4764	.5099	.5320	.4713	.3659	.5390	.5230	.5207
2.508	.4751	.3607	.2568	.3448	.2935	.4297	.4977	.4248
2.989	.4773	.3616	.2541	.1683	.2119	.2724	.3125	.3533
4.047	.4854	.3637	.2552	.1694	.0927	.1765	.1730	.1797
4.999	.4889	.3641	.2557	.1696	.0925	.0715	.0995	.1167

TABLE IX. Concluded

(b) Sidewall pressures

NPR	PRSID1	PRSID2	PRSID3	PRSID4	PRSID5	PRSID6	PRSID7	PRSID9	PRSID10	PRSID11
2.015	.8694	.8618	.8398	.8753	.8148	.7589	.8849	.4337	.4214	.4190
2.508	.8646	.8559	.8313	.8712	.8063	.7541	.8836	.4282	.4184	.4151
2.989	.8629	.8541	.8265	.8697	.8034	.7529	.8830	.4267	.4196	.4147
4.047	.8625	.8529	.8261	.8691	.8016	.7529	.8829	.4254	.4231	.4159
4.999	.8622	.8523	.8225	.8683	.8006	.7526	.8831	.4260	.4246	.4158

NPR	PRSID13	PRSID14	PRSID15	PRSID16	PRSID17	PRSID18	PRSID19	PRSID20	PRSID21	PRSID22
2.015	.4880	.4918	.5243	.5262	.9372	.8998	.9327	.8470	.8582	.7800
2.508	.3738	.3563	.2629	.2453	.9349	.8962	.9294	.8404	.8521	.7689
2.989	.2943	.2262	.2466	.2436	.9341	.8949	.9283	.8381	.8501	.7650
4.047	.1619	.2120	.2471	.2423	.9324	.8933	.9267	.8363	.8489	.7632
4.999	.1385	.2117	.2475	.2368	.9310	.8924	.9256	.8350	.8483	.7628

NPR	PRSID23	PRSID24	PRSID25	PRSID27	PRSID28	PRSID29	PRSID30	PRSID31	PRSID33	PRSID36
2.015	.7702	.7494	.7197	.7104	.6263	.5114	.5870	.4956	.4953	.5181
2.508	.7575	.7342	.7004	.6935	.5902	.4222	.5512	.3982	.3980	.4174
2.989	.7537	.7291	.6953	.6878	.5716	.3644	.5378	.3338	.3338	.3502
4.047	.7523	.7267	.6939	.6843	.5530	.2868	.5305	.2466	.2464	.2716
4.999	.7531	.7265	.6932	.6838	.5507	.2475	.5300	.1995	.1994	.2342

TABLE X. RATIO OF INTERNAL STATIC PRESSURE TO JET TOTAL PRESSURE FOR CONFIGURATION 9

(a) Flap pressures

Upper flap pressures

NPR	$x'/l_{u,rot}$							
	-1.396	-.823	-.537	-.251	.178	.392	.606	.819
2.003	.8859	.9160	.9393	.9387	.9369	.9139	.8895	.8101
2.500	.8835	.9142	.9411	.9372	.9354	.9124	.8874	.8041
3.037	.8839	.9144	.9447	.9379	.9363	.9132	.8882	.8039
4.004	.8842	.9146	.9492	.9395	.9381	.9152	.8915	.8049
4.507	.8840	.9140	.9508	.9399	.9388	.9155	.8930	.8052

Fixed lower flap pressures

NPR	$x'/l_{l,fixed}$			
	.385	.605	.846	.969
2.003	.7832	.6825	.3880	.4763
2.500	.7793	.6768	.2542	.3711
3.037	.7793	.6759	.2215	.2706
4.004	.7800	.6755	.2219	.1981
4.507	.7798	.6749	.2210	.1956

Lower rotating flap pressures

Top

NPR	$x''/l_{l,rot}$							
	.131	.242	.353	.463	.574	.685	.796	.906
2.003	.5204	.6585	.6209	.5301	.4166	.4588	.5422	.5363
2.500	.4955	.6396	.5936	.5014	.3529	.3319	.3166	.3674
3.037	.4927	.6347	.5812	.4860	.3225	.2852	.2616	.2226
4.004	.5010	.6344	.5769	.4788	.3033	.2497	.2186	.1757
4.507	.5065	.6344	.5761	.4784	.3022	.2466	.2092	.1633

Bottom

NPR	$x''/l_{l,rot}$							
	.131	.242	.353	.463	.574	.685	.796	.906
2.003	.7212	.6271	.5593	.4829	.3616	.4434	.5551	.5384
2.500	.7059	.5879	.4714	.3614	.2837	.2647	.2969	.4422
3.037	.7066	.5875	.4622	.3317	.1943	.1855	.2729	.2868
4.004	.7083	.5886	.4639	.3320	.1947	.1520	.1207	.0964
4.507	.7085	.5883	.4642	.3315	.1946	.1519	.1206	.0966

TABLE X. Concluded

(b) Sidewall pressures

NPR	PRSID1	PRSID2	PRSID3	PRSID4	PRSID5	PRSID6	PRSID7	PRSID9	PRSID10	PRSID11
2.003	.8625	.8647	.8144	.8497	.8578	.7329	.8152	.5065	.5898	.6056
2.500	.8582	.8609	.8102	.8458	.8533	.7269	.8104	.4720	.5496	.5646
3.037	.8579	.8603	.8101	.8452	.8520	.7263	.8104	.4702	.5495	.5641
4.004	.8584	.8604	.8105	.8452	.8514	.7268	.8107	.4688	.5499	.5642
4.507	.8579	.8600	.8099	.8451	.8509	.7264	.8107	.4679	.5494	.5643

NPR	PRSID13	PRSID14	PRSID15	PRSID16	PRSID17	PRSID18	PRSID19	PRSID20	PRSID21	PRSID22
2.003	.4634	.4983	.5252	.5333	.9331	.8861	.9302	.7912	.8365	.6792
2.500	.3774	.4221	.4344	.4325	.9321	.8833	.9286	.7828	.8308	.6606
3.037	.2551	.3174	.3917	.4183	.9317	.8827	.9279	.7808	.8298	.6563
4.004	.2042	.3147	.3922	.4185	.9303	.8814	.9264	.7799	.8302	.6576
4.507	.1997	.3137	.3919	.4184	.9296	.8805	.9260	.7796	.8302	.6585

NPR	PRSID23	PRSID24	PRSID25	PRSID27	PRSID28	PRSID29	PRSID30	PRSID31	PRSID33	PRSID36
2.003	.6883	.6865	.6393	.6261	.5454	.4990	.5330	.4977	.4988	.4994
2.500	.6694	.6657	.6142	.5952	.4799	.3995	.4960	.3991	.3995	.4029
3.037	.6652	.6616	.6101	.5829	.4407	.3294	.4734	.3290	.3287	.3363
4.004	.6651	.6622	.6082	.5800	.4084	.2530	.4602	.2495	.2493	.2645
4.507	.6663	.6625	.6096	.5799	.4136	.2262	.4585	.2214	.2211	.2370

TABLE XI. RATIO OF INTERNAL STATIC PRESSURE TO JET TOTAL PRESSURE FOR CONFIGURATION 10

(a) Flap pressures

Upper flap pressures

NPR	$x'/l_{u,rot}$							
	-1.396	-.823	-.537	-.251	.178	.392	.606	.819
1.990	.8701	.8973	.9230	.9227	.9001	.8633	.8350	.7271
2.485	.8664	.8945	.9237	.9207	.8967	.8566	.8281	.7155
3.030	.8670	.8946	.9274	.9215	.8974	.8572	.8289	.7158
3.503	.8672	.8946	.9296	.9220	.8978	.8573	.8298	.7156

Fixed lower flap pressures

NPR	$x'/l_{l,fixed}$			
	.385	.605	.846	.969
1.990	.7735	.6742	.3112	.4675
2.485	.7670	.6659	.2280	.3583
3.030	.7673	.6650	.2256	.2731
3.503	.7676	.6644	.2254	.2651

Lower rotating flap pressures

Top

NPR	$x''/l_{l,rot}$							
	.131	.242	.353	.463	.574	.685	.796	.906
1.990	.2811	.2877	.3466	.4259	.4791	.5137	.5380	.5499
2.485	.1760	.2136	.3296	.3475	.2253	.4070	.4747	.4613
3.030	.1750	.2100	.3293	.3495	.2229	.1816	.2850	.3237
3.503	.1746	.2078	.3300	.3511	.2238	.1817	.1554	.1190

Bottom

NPR	$x''/l_{l,rot}$							
	.131	.242	.353	.463	.574	.685	.796	.906
1.990	.8799	.7927	.6999	.5625	.4340	.4487	.5488	.5168
2.485	.8733	.7755	.6681	.5251	.3765	.3448	.2998	.3998
3.030	.8737	.7748	.6668	.5114	.3254	.2678	.2607	.2440
3.503	.8748	.7749	.6679	.5114	.3254	.2664	.2354	.2134

TABLE XI. Concluded

(b) Sidewall pressures

NPR	PRSID1	PRSID2	PRSID3	PRSID4	PRSID5	PRSID6	PRSID7	PRSID8	PRSID9	PRSID10	PRSID11
1.990	.8518	.8738	.8255	.8396	.9024	.7266	.8193	.8493	.5419	.6606	.7164
2.485	.8469	.8703	.8073	.8336	.8985	.7178	.8113	.8379	.5081	.6257	.6879
3.030	.8471	.8706	.7992	.8337	.8996	.7176	.8109	.8376	.5055	.6242	.6856
3.503	.8474	.8709	.7914	.8335	.8993	.7175	.8108	.8373	.5039	.6237	.6853

NPR	PRSID12	PRSID13	PRSID14	PRSID15	PRSID16	PRSID17	PRSID18	PRSID19	PRSID20	PRSID21	PRSID22
1.990	.7667	.4638	.5502	.5999	.6318	.9033	.8339	.8610	.6032	.7389	.3385
2.485	.7433	.3964	.4738	.5468	.5898	.9001	.8275	.8543	.5849	.7238	.2869
3.030	.7413	.2939	.4251	.5277	.5768	.8000	.8275	.8538	.5843	.7240	.2847
3.503	.7411	.2817	.4215	.5273	.5767	.8993	.8270	.8535	.5834	.7230	.2838

NPR	PRSID23	PRSID24	PRSID25	PRSID26	PRSID27	PRSID28	PRSID29	PRSID30	PRSID31	PRSID33	PRSID36
1.990	.4876	.5696	.6014	.5173	.3334	.4008	.5141	.4616	.5010	.5010	.5045
2.485	.4628	.5501	.5844	.4567	.2501	.3406	.4133	.3394	.4011	.4013	.4122
3.030	.4603	.5462	.5836	.4334	.2471	.3368	.3345	.3318	.3294	.3292	.3470
3.503	.4590	.5474	.5843	.4286	.2458	.3370	.2844	.3319	.2857	.2849	.2957

TABLE XII. RATIO OF INTERNAL STATIC PRESSURE TO JET TOTAL PRESSURE FOR CONFIGURATION 11

(a) Flap pressures

Upper flap pressures

NPR	$x'/l_{u,rot}$									
	-1.396	-.823	-.537	-.251	.178	.392	.607	.821	1.035	1.249
2.004	.8675	.8767	.8973	.8780	.7457	.7374	.7180	.6875	.6501	.5681
2.493	.8659	.8752	.8991	.8766	.7410	.7328	.7127	.6808	.6426	.5615
3.030	.8660	.8746	.9019	.8763	.7395	.7318	.7120	.6796	.6419	.5620
3.997	.8653	.8738	.9054	.8765	.7380	.7312	.7119	.6787	.6414	.5637
5.039	.8645	.8721	.9076	.8761	.7366	.7303	.7120	.6783	.6406	.5634

Fixed lower flap pressures

NPR	$x'/l_{l,fixed}$		
	.385	.605	.846
2.004	.8604	.8588	.8863
2.493	.8588	.8568	.8847
3.030	.8582	.8561	.8842
3.997	.8575	.8547	.8839
5.039	.8566	.8527	.8827

Lower rotating flap pressures

Top

NPR	$x''/l_{l,rot}$							
	.131	.242	.353	.463	.574	.685	.796	.906
2.004	.8681	.8415	.8173	.7778	.7579	.7394	.7155	.6514
2.493	.8675	.8391	.8145	.7750	.7534	.7353	.7101	.6466
3.030	.8676	.8385	.8136	.7740	.7512	.7340	.7082	.6448
3.997	.8674	.8386	.8123	.7721	.7487	.7323	.7058	.6445
5.039	.8659	.8382	.8106	.7696	.7470	.7307	.7043	.6424

TABLE XII. Concluded

(b) Sidewall pressures

NPR	PRSID1	PRSID2	PRSID3	PRSID4	PRSID5	PRSID6	PRSID7	PRSID8	PRSID9	PRSID10	PRSID11
2.004	.8599	.8512	.8669	.8572	.8463	.8650	.8598	.8410	.8761	.8669	.8492
2.493	.8580	.8492	.8619	.8552	.8441	.8630	.8583	.8390	.8742	.8648	.8471
3.030	.8571	.8485	.8576	.8546	.8433	.8624	.8576	.8378	.8738	.8646	.8466
3.997	.8562	.8476	.8554	.8532	.8425	.8619	.8563	.8362	.8742	.8648	.8459
5.039	.8548	.8461	.8534	.8514	.8415	.8609	.8551	.8350	.8735	.8635	.8447

NPR	PRSID12	PRSID17	PRSID18	PRSID19	PRSID20	PRSID21	PRSID22	PRSID23	PRSID24	PRSID25	PRSID26
2.004	.8327	.8414	.8232	.7771	.8200	.7811	.7999	.7812	.7668	.7495	.7331
2.493	.8304	.8395	.8207	.7737	.8178	.7778	.7965	.7766	.7624	.7453	.7288
3.030	.8297	.8387	.8196	.7727	.8170	.7767	.7954	.7758	.7612	.7444	.7283
3.997	.8284	.8370	.8178	.7713	.8154	.7748	.7942	.7755	.7600	.7430	.7274
5.039	.8271	.8351	.8151	.7694	.8140	.7733	.7932	.7761	.7584	.7417	.7254

NPR	PRSID27	PRSID28	PRSID29	PRSID30	PRSID31	PRSID32	PRSID33	PRSID34	PRSID35	PRSID36	PRSID37
2.004	.7822	.7353	.7079	.7699	.6563	.6123	.6507	.6055	.5521	.6423	.5867
2.493	.7787	.7352	.7014	.7650	.6485	.6005	.6406	.5845	.5116	.6301	.5382
3.030	.7777	.7353	.6993	.7636	.6473	.5991	.6394	.5824	.5014	.6297	.5276
3.997	.7767	.7314	.6983	.7622	.6465	.5988	.6384	.5816	.5009	.6297	.5290
5.039	.7754	.7533	.6975	.7603	.6431	.5986	.6374	.5814	.5009	.6288	.5294

TABLE XIII. RATIO OF INTERNAL STATIC PRESSURE TO JET TOTAL PRESSURE FOR CONFIGURATION 12

(a) Flap pressures

Upper flap pressures

NPR	$x'/l_{u,rot}$									
	-1.396	-.823	-.537	-.251	.178	.392	.607	.821	1.035	1.249
2.001	.9119	.9322	.9532	.9487	.9377	.9146	.8840	.8472	.7977	.6863
2.496	.9092	.9301	.9550	.9476	.9354	.9112	.8791	.8402	.7887	.6747
3.018	.9091	.9294	.9581	.9475	.9348	.9105	.8783	.8386	.7864	.6735
4.042	.9091	.9287	.9620	.9481	.9348	.9106	.8796	.8376	.7850	.6732
5.027	.9086	.9270	.9629	.9481	.9346	.9107	.8814	.8373	.7841	.6724

Fixed lower flap pressures

NPR	$x'/l_{l,fixed}$			
	.385	.605	.846	.969
2.001	.8530	.7936	.3620	.4933
2.496	.8507	.7904	.3523	.3751
3.018	.8503	.7901	.3535	.3102
4.042	.8501	.7889	.3528	.1477
5.027	.8497	.7882	.3525	.1428

Fixed lower flap pressures

Top

NPR	$x''/l_{l,rot}$							
	.131	.242	.353	.463	.574	.685	.796	.906
2.001	.8195	.8263	.8117	.7679	.7385	.7055	.6637	.5912
2.496	.8124	.8187	.8040	.7570	.7236	.6855	.6346	.5510
3.018	.8109	.8171	.8017	.7540	.7188	.6789	.6229	.5322
4.042	.8093	.8164	.8001	.7520	.7157	.6764	.6193	.5268
5.027	.8078	.8164	.7989	.7500	.7143	.6749	.6173	.5253

Bottom

NPR	$x''/l_{l,rot}$							
	.131	.242	.353	.463	.574	.685	.796	.906
2.001	.3321	.3472	.5020	.5237	.5077	.5139	.5102	.5190
2.496	.1954	.2796	.3956	.4268	.4184	.4157	.4119	.4180
3.018	.1917	.1293	.2352	.3209	.3801	.3418	.3733	.3298
4.042	.1824	.1302	.1244	.1815	.1971	.2205	.2482	.2768
5.027	.1833	.1306	.0891	.1613	.1639	.1645	.1744	.1930

TABLE XIII. Concluded

(b) Sidewall pressures

NPR	PRSID1	PRSID2	PRSID3	PRSID4	PRSID5	PRSID6	PRSID7	PRSID8	PRSID9
2.001	.8947	.8922	.8762	.8855	.8775	.8446	.8920	.8472	.4904
2.496	.8915	.8884	.8754	.8822	.8729	.8420	.8871	.8404	.4757
3.018	.8907	.8874	.8746	.8810	.8718	.8418	.8862	.8379	.4660
4.042	.8904	.8867	.8769	.8804	.8708	.8421	.8873	.8347	.4510
5.027	.8904	.8862	.8757	.8794	.8701	.8423	.8852	.8328	.4424

NPR	PRSID10	PRSID12	PRSID13	PRSID14	PRSID15	PRSID17	PRSID18	PRSID19	PRSID20
2.001	.3175	.8373	.4913	.4960	.5127	.9371	.9103	.9193	.8817
2.496	.2707	.8301	.3869	.3859	.3902	.9362	.9076	.9164	.8776
3.018	.2625	.8284	.3236	.2717	.2750	.9363	.9075	.9159	.8766
4.042	.2616	.8272	.2696	.1968	.1307	.9360	.9068	.9151	.8754
5.027	.2517	.8253	.2159	.1526	.1144	.9348	.9060	.9142	.8743

NPR	PRSID21	PRSID22	PRSID23	PRSID24	PRSID25	PRSID26	PRSID27	PRSID28	PRSID29
2.001	.8764	.8448	.8363	.8324	.8264	.8319	.8042	.7793	.7365
2.496	.8719	.8381	.8298	.8254	.8188	.8252	.7951	.7683	.7226
3.018	.8709	.8366	.8286	.8239	.8170	.8240	.7927	.7670	.7199
4.042	.8700	.8356	.8293	.8235	.8157	.8232	.7912	.7655	.7184
5.027	.8693	.8354	.8303	.8232	.8145	.8225	.7903	.7648	.7178

NPR	PRSID30	PRSID31	PRSID32	PRSID33	PRSID34	PRSID35	PRSID36	PRSID37
2.001	.7357	.4989	.4989	.4986	.4991	.4990	.5793	.5418
2.496	.7196	.4000	.3998	.3996	.4000	.3999	.5070	.4387
3.018	.7151	.3306	.3305	.3304	.3309	.3305	.4463	.3757
4.042	.7121	.2469	.2466	.2467	.2469	.2466	.3962	.2999
5.027	.7107	.1984	.1984	.1982	.1985	.1982	.3927	.2549

TABLE XIV. RATIO OF INTERNAL STATIC PRESSURE TO JET TOTAL PRESSURE FOR CONFIGURATION 13

(a) Flap pressures

Upper flap pressures

NPR	$x'/l_{u,rot}$									
	-1.396	-.823	-.537	-.251	.178	.392	.607	.821	1.035	1.249
2.022	.9140	.9377	.9567	.9520	.9538	.9331	.9028	.8644	.8111	.6940
2.535	.9125	.9365	.9601	.9524	.9531	.9313	.8992	.8602	.8049	.6850
3.024	.9122	.9363	.9626	.9529	.9531	.9307	.8988	.8585	.8029	.6837
4.017	.9123	.9360	.9670	.9543	.9539	.9312	.9003	.8582	.8017	.6843
5.019	.9114	.9342	.9673	.9544	.9540	.9309	.9018	.8573	.8005	.6831

Fixed lower flap pressures

NPR	$x'/l_{l,fixed}$			
	.385	.605	.846	.969
2.022	.8189	.7247	.4112	.4835
2.535	.8179	.7226	.2788	.3729
3.024	.8176	.7213	.2592	.2984
4.017	.8177	.7205	.2600	.1589
5.019	.8169	.7191	.2595	.1509

Lower rotating flap pressures

Top

NPR	$x''/l_{l,rot}$							
	.131	.242	.353	.463	.574	.685	.796	.906
2.022	.7948	.7981	.7691	.6937	.6329	.5812	.5412	.4928
2.535	.7896	.7919	.7617	.6804	.6080	.5412	.4720	.3929
3.024	.7876	.7896	.7591	.6758	.5981	.5241	.4468	.3582
4.017	.7869	.7895	.7583	.6742	.5960	.5211	.4308	.3243
5.019	.7849	.7887	.7568	.6722	.5946	.5207	.4305	.3235

Bottom

NPR	$x''/l_{l,rot}$							
	.131	.242	.353	.463	.574	.685	.796	.906
2.022	.4715	.4341	.5444	.4721	.3638	.5351	.5251	.5181
2.535	.4726	.3665	.2594	.3545	.2735	.4157	.4979	.4362
3.024	.4780	.3686	.2590	.1720	.2138	.2565	.2955	.3341
4.017	.4834	.3698	.2594	.1727	.0939	.1801	.1772	.1916
5.019	.4872	.3703	.2596	.1725	.0935	.0727	.0578	.1056

TABLE XIV. Concluded

(b) Sidewall pressures

NPR	PRSID1	PRSID2	PRSID3	PRSID4	PRSID5	PRSID6	PRSID7	PRSID9	PRSID10
2.022	.8920	.8909	.8558	.8917	.8660	.7816	.8734	.5289	.4642
2.535	.8904	.8887	.8535	.8900	.8622	.7788	.8748	.5075	.4502
3.024	.8896	.8876	.8524	.8888	.8600	.7776	.8744	.4965	.4474
4.017	.8897	.8873	.8521	.8881	.8590	.7774	.8744	.4811	.4436
5.019	.8892	.8863	.8511	.8873	.8568	.7764	.8753	.4767	.4429

NPR	PRSID11	PRSID13	PRSID14	PRSID15	PRSID16	PRSID17	PRSID18	PRSID19
2.022	.4612	.4858	.4996	.5168	.5351	.9456	.9130	.9485
2.535	.4479	.3876	.3631	.3074	.2940	.9465	.9126	.9480
3.024	.4460	.3139	.2748	.2610	.2750	.9467	.9126	.9475
4.017	.4426	.2178	.2033	.2546	.2729	.9467	.9124	.9474
5.019	.4418	.1548	.2019	.2542	.2732	.9453	.9123	.9463

NPR	PRSID20	PRSID21	PRSID22	PRSID23	PRSID24	PRSID25	PRSID27	PRSID28	PRSID29
2.022	.8759	.8873	.8266	.8156	.8261	.8433	.7732	.7418	.4937
2.535	.8743	.8850	.8230	.8115	.8210	.8382	.7665	.7328	.3937
3.024	.8736	.8838	.8218	.8107	.8194	.8363	.7645	.7307	.3300
4.017	.8732	.8833	.8221	.8115	.8198	.8351	.7648	.7301	.2484
5.019	.8723	.8814	.8218	.8134	.8180	.8331	.7642	.7282	.1987

NPR	PRSID30	PRSID31	PRSID32	PRSID33	PRSID34	PRSID35	PRSID36	PRSID37
2.022	.6779	.4942	.4941	.4938	.4944	.4941	.4939	.4941
2.535	.6621	.3940	.3939	.3939	.3942	.3941	.3935	.3939
3.024	.6573	.3302	.3302	.3299	.3303	.3301	.3303	.3301
4.017	.6562	.2485	.2486	.2484	.2487	.2487	.2512	.2484
5.019	.6553	.1989	.1990	.1989	.1989	.1989	.2073	.1992

TABLE XV. RATIO OF INTERNAL STATIC PRESSURE TO JET TOTAL PRESSURE FOR CONFIGURATION 14

(a) Flap pressures

Upper flap pressures

NPR	$x'/l_{u,rot}$									
	-1.396	-.823	-.537	-.251	.178	.392	.607	.821	1.035	1.249
2.027	.9011	.9295	.9510	.9483	.9477	.9200	.8774	.8274	.7655	.6480
2.489	.9001	.9286	.9532	.9480	.9469	.9197	.8764	.8249	.7626	.6443
3.009	.8999	.9284	.9563	.9484	.9470	.9199	.8767	.8241	.7611	.6442
4.021	.8997	.9279	.9613	.9499	.9484	.9207	.8782	.8235	.7600	.6438
4.474	.8996	.9275	.9624	.9502	.9486	.9211	.8793	.9237	.7598	.6437

Fixed lower flap pressures

NPR	$x'/l_{l,fixed}$			
	.385	.605	.846	.969
2.027	.7952	.6942	.3691	.4704
2.489	.7930	.6907	.2589	.3714
3.009	.7929	.6895	.2397	.2687
4.021	.7934	.6888	.2401	.2072
4.474	.7933	.6885	.2399	.2072

Lower rotating flap pressures

Top

NPR	$x''/l_{l,rot}$							
	.131	.242	.353	.463	.574	.685	.796	.906
2.027	.6816	.7189	.6762	.5739	.4813	.4810	.5215	.5152
2.489	.6862	.7138	.6703	.5673	.4349	.3877	.3502	.3104
3.009	.6893	.7116	.6688	.5662	.4228	.3501	.3004	.2503
4.021	.6875	.7089	.6664	.5647	.4203	.3451	.2746	.2006
4.474	.6884	.7085	.6660	.5646	.4199	.3452	.2743	.1993

Bottom

NPR	$x''/l_{l,rot}$							
	.131	.242	.353	.463	.574	.685	.796	.906
2.027	.7133	.6189	.5529	.4766	.3550	.3966	.5531	.5394
2.489	.7013	.5874	.4672	.3802	.2905	.2709	.3128	.4461
3.009	.7025	.5882	.4649	.3350	.1955	.1538	.2629	.2908
4.021	.7066	.5915	.4676	.3362	.1963	.1547	.1226	.0977
4.474	.7074	.5920	.4672	.3364	.1955	.1549	.1227	.0981

TABLE XV. Concluded

(b) Sidewall pressures

NPR	PRSID1	PRSID2	PRSID3	PRSID4	PRSID5	PRSID6	PRSID7	PRSID9	PRSID10
2.027	.8781	.8850	.8291	.8608	.8863	.7500	.8203	.5706	.6001
2.489	.8764	.8832	.8268	.8581	.8842	.7451	.8161	.5417	.5707
3.009	.8755	.8821	.8263	.8575	.8828	.7437	.8156	.5281	.5672
4.021	.8748	.8808	.8264	.8568	.8816	.7437	.8156	.5183	.5649
4.474	.8748	.8805	.8264	.8565	.3811	.7437	.8155	.5160	.5642

NPR	PRSID11	PRSID13	PRSID14	PRSID15	PRSID16	PRSID17	PRSID18	PRSID19
2.027	.6220	.4751	.4953	.5178	.5459	.9432	.8955	.9438
2.489	.5928	.3727	.4059	.4249	.4480	.9429	.8956	.9430
3.009	.5913	.2964	.3341	.4020	.4412	.9426	.8950	.9427
4.021	.5930	.2078	.3161	.4025	.4425	.9415	.8917	.9406
4.474	.5923	.1914	.3175	.4024	.4426	.9411	.8919	.9404

NPR	PRSID20	PRSID21	PRSID22	PRSID23	PRSID24	PRSID25	PRSID27	PRSID28	PRSID29
2.027	.8257	.8585	.7398	.7474	.7804	.8006	.6934	.6877	.4926
2.489	.8230	.8565	.7365	.7429	.7771	.7975	.6877	.6542	.4016
3.009	.8221	.8559	.7368	.7424	.7766	.7968	.6864	.6533	.3323
4.021	.8198	.8551	.7343	.7396	.7751	.7950	.6840	.6620	.2484
4.474	.8193	.8546	.7342	.7404	.7747	.7945	.6840	.6612	.2233

NPR	PRSID30	PRSID31	PRSID32	PRSID33	PRSID34	PRSID35	PRSID36	PRSID37
2.027	.5975	.4928	.4929	.4929	.4933	.4927	.4924	.4929
2.489	.5829	.4018	.4018	.4017	.4015	.4016	.4020	.4017
3.009	.5793	.3323	.3324	.3323	.3322	.3322	.3325	.3322
4.021	.5776	.2484	.2485	.2484	.2481	.2484	.2487	.2484
4.474	.5775	.2232	.2231	.2231	.2231	.2230	.2235	.2232

TABLE XVI. RATIO OF INTERNAL STATIC PRESSURE TO JET TOTAL PRESSURE FOR CONFIGURATION 15

(a) Flap pressures

Upper flap pressures

NPR	$x'/l_{u,rot}$									
	-1.396	-.823	-.537	-.251	.178	.392	.607	.821	1.035	1.249
1.982	.8767	.9039	.9286	.9281	.9112	.8502	.7666	.6607	.5535	.4411
2.491	.8727	.9008	.9296	.9260	.9076	.8413	.7484	.6260	.5008	.3788
2.986	.8732	.9012	.9330	.9269	.9080	.8414	.7486	.6253	.5002	.3795
3.496	.8735	.9011	.9358	.9275	.9082	.8415	.7486	.6246	.4996	.3796

Fixed lower flap pressures

NPR	$x'/l_{l,fixed}$			
	.385	.605	.846	.969
1.982	.7794	.6798	.3063	.4688
2.491	.7724	.6707	.2337	.3572
2.986	.7726	.6701	.2318	.2790
3.496	.7726	.6694	.2319	.2699

Lower rotating flap pressures

Top

NPR	$x''/l_{l,rot}$							
	.131	.242	.353	.463	.574	.685	.796	.906
1.982	.3236	.3298	.3640	.4147	.4503	.4781	.5011	.5169
2.491	.1228	.1964	.2929	.3232	.2420	.4350	.4772	.4424
2.986	.1169	.1938	.2936	.3244	.2406	.2208	.2129	.3681
3.496	.1170	.1910	.2935	.3251	.2407	.2204	.2089	.1715

Bottom

NPR	$x''/l_{l,rot}$							
	.131	.242	.353	.463	.574	.685	.796	.906
1.982	.8771	.7905	.6988	.5620	.4350	.4700	.5452	.5145
2.491	.8702	.7735	.6678	.5264	.3783	.3451	.2963	.3957
2.986	.8704	.7731	.6664	.5124	.3266	.2693	.2688	.2479
3.496	.8708	.7733	.6675	.5127	.3269	.2682	.2383	.2164

TABLE XVI. Concluded

(b) Sidewall pressures

NPR	PRSID1	PRSID2	PRSID3	PRSID4	PRSID5	PRSID6	PRSID7	PRSID8	PRSID9	PRSID10
1.982	.8581	.8785	.8117	.8433	.9064	.7354	.8224	.8514	.5990	.6747
2.491	.8524	.8740	.8037	.8366	.9015	.7250	.8136	.8395	.5596	.6401
2.986	.8526	.8743	.8037	.8362	.9024	.7244	.8131	.8386	.5468	.6360
3.496	.8525	.8745	.8037	.8363	.9028	.7242	.8127	.8385	.5412	.6346

NPR	PRSID11	PRSID12	PRSID13	PRSID14	PRSID15	PRSID16	PRSID17	PRSID18	PRSID19
1.982	.7306	.7700	.4666	.5498	.6039	.6458	.9117	.8380	.8580
2.491	.7042	.7466	.3638	.4606	.5433	.6059	.9084	.8314	.8504
2.986	.7014	.7440	.3125	.4253	.5316	.5954	.9088	.8316	.8505
3.496	.7011	.7436	.2716	.4178	.5310	.5952	.9077	.8308	.8498

NPR	PRSID20	PRSID21	PRSID22	PRSID23	PRSID24	PRSID25	PRSID26	PRSID27	PRSID28
1.982	.6140	.7072	.3597	.4712	.5417	.5765	.5768	.3796	.4097
2.491	.5939	.6861	.1614	.3724	.4846	.5341	.5388	.2622	.3101
2.986	.5947	.6859	.1750	.3700	.4841	.5332	.5363	.2565	.3087
3.496	.5939	.6852	.1762	.3682	.4836	.5327	.5342	.2596	.3124

NPR	PRSID29	PRSID30	PRSID31	PRSID32	PRSID33	PRSID34	PRSID35	PRSID36	PRSID37
1.982	.4497	.4389	.5040	.5039	.5035	.5039	.5039	.5038	.5040
2.491	.3795	.3494	.4011	.4009	.4007	.4009	.4010	.4008	.4010
2.986	.3803	.3233	.3346	.3345	.3343	.3346	.3346	.3343	.3345
3.496	.3810	.3226	.2858	.2857	.2854	.2856	.2857	.2855	.2855

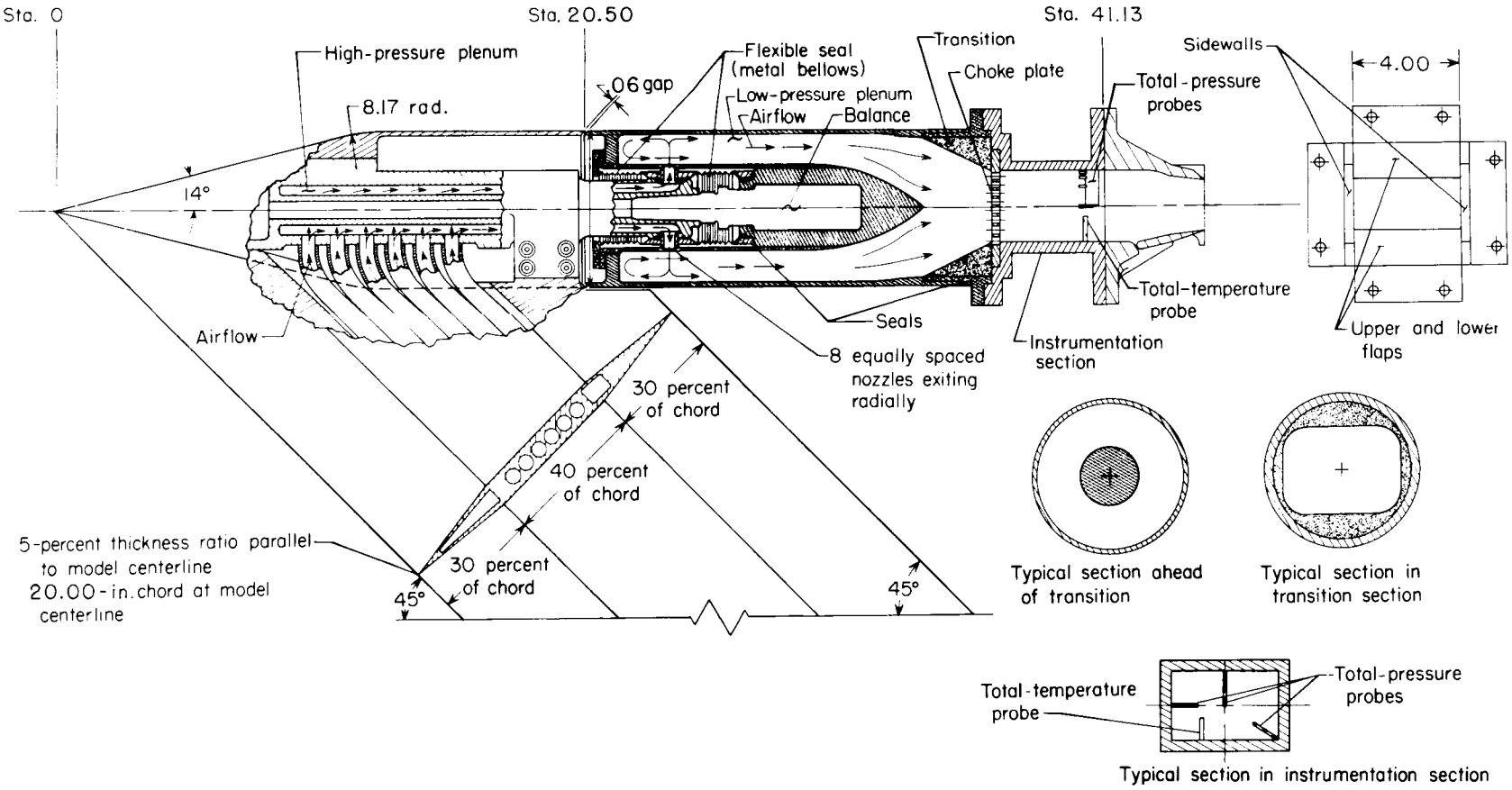

Figure 1. Sketch of air-powered nacelle model with convergent nonaxisymmetric nozzle installed. All dimensions are in inches unless otherwise noted.

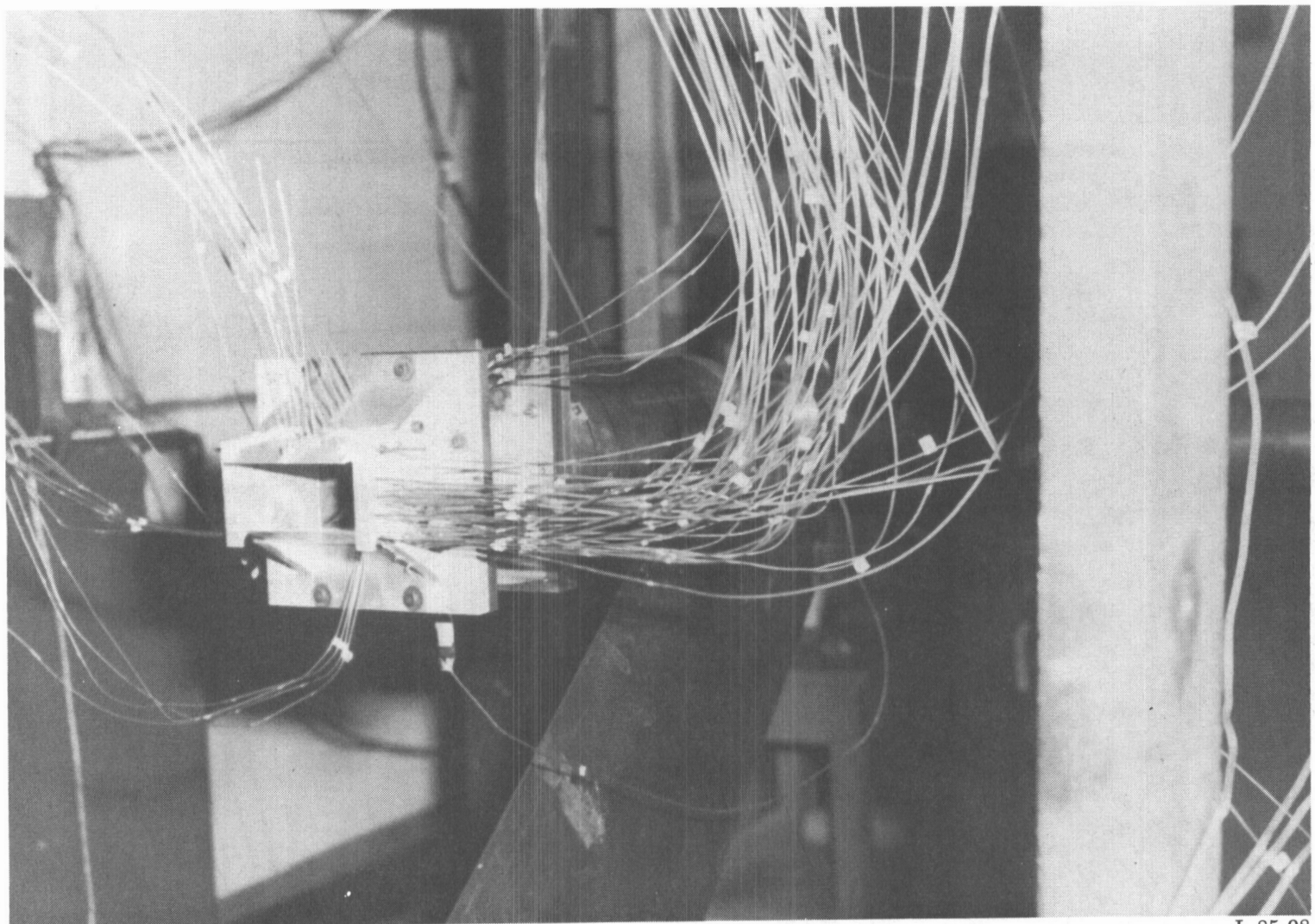

L-85-08

(a) Convergent two-dimensional nozzle installed on single-engine propulsion system in static-test facility of Langley 16-Foot Transonic Tunnel.

Figure 2. Model photographs.

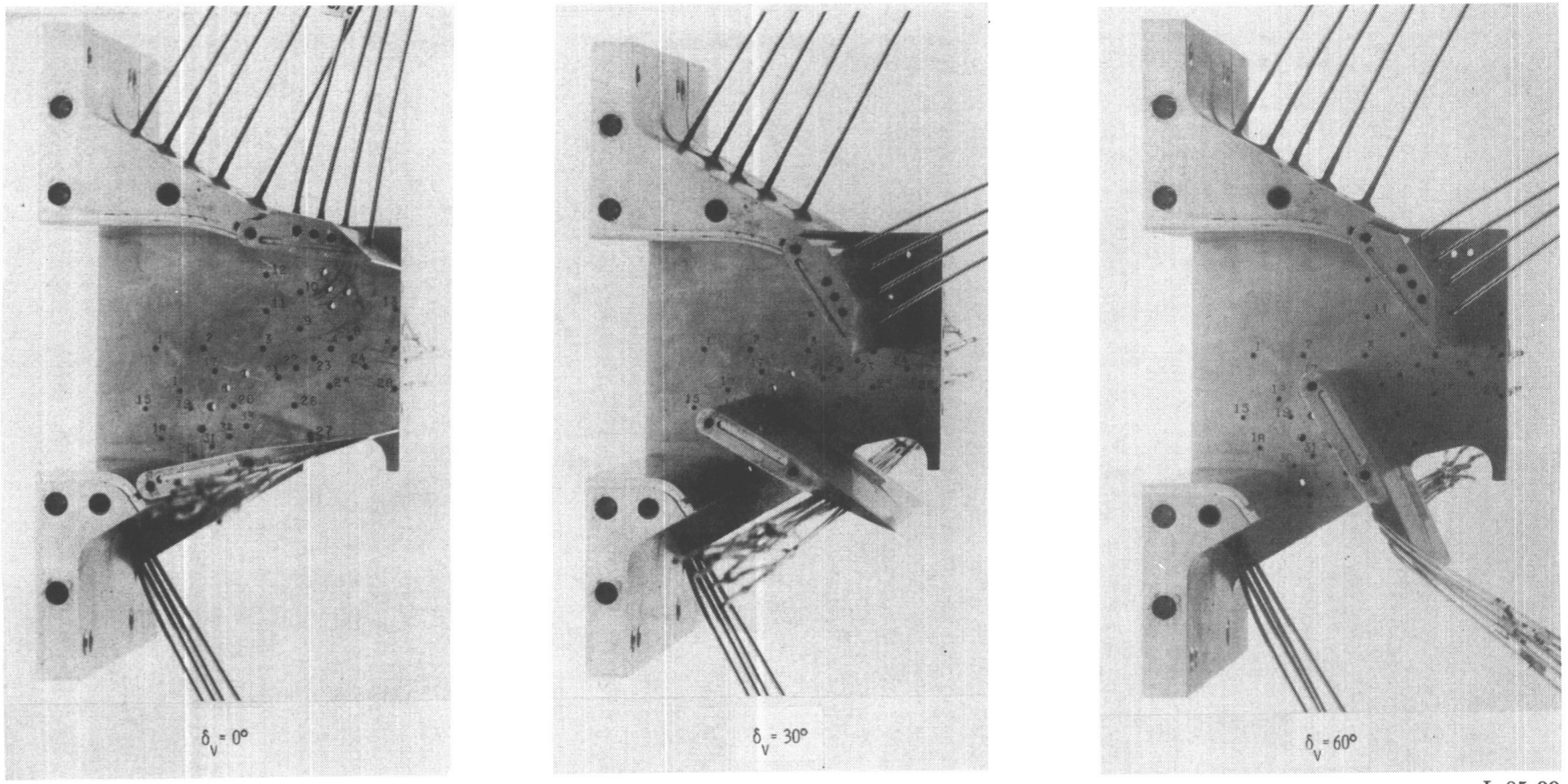

L-85-09

(b) Side views with left-hand sidewall removed, baseline upper rotating flap.

Figure 2. Concluded.

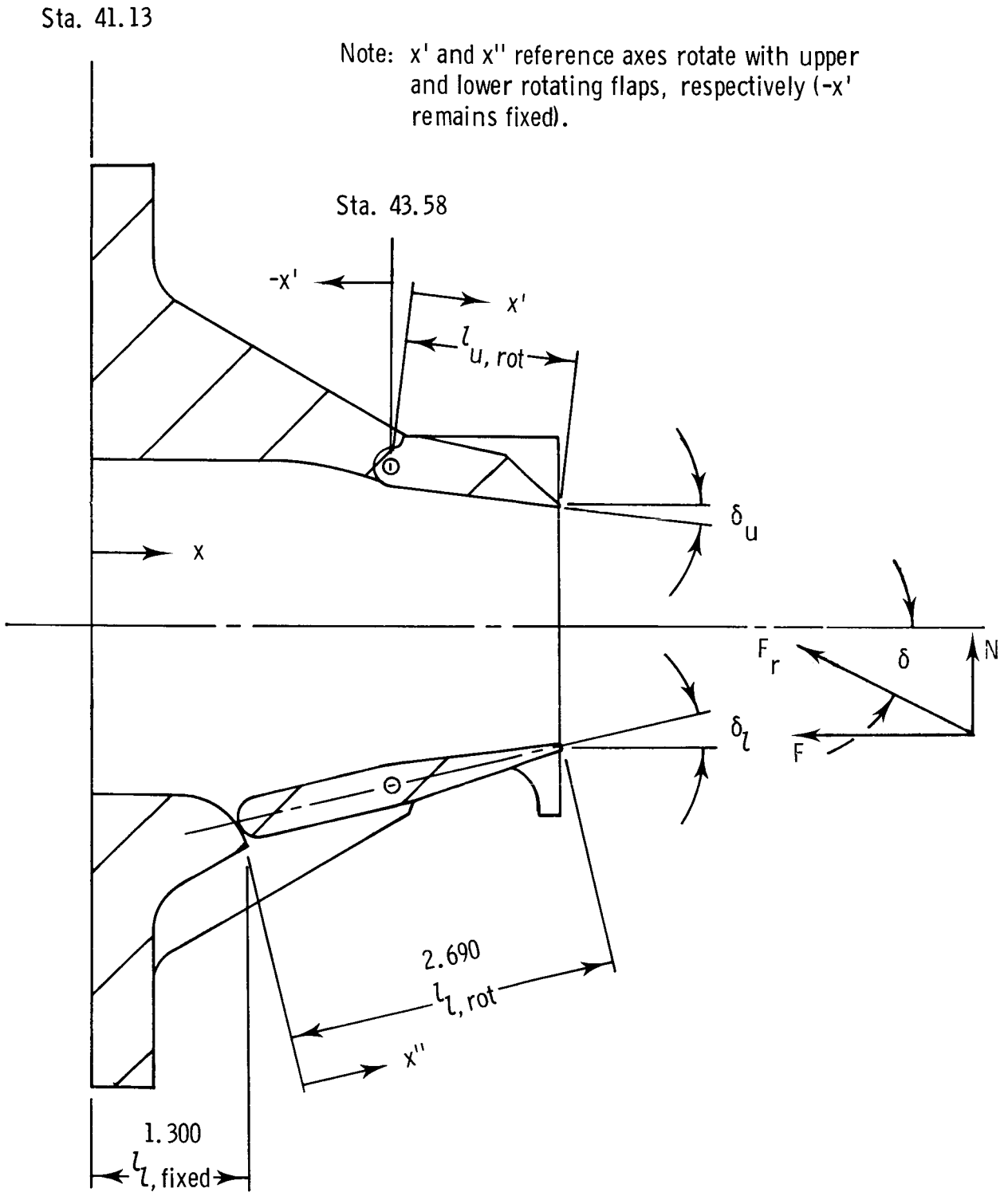

(a) Reference axes and other nozzle parameters.

Figure 3. Sketches defining nozzle geometry and important model parameters. All dimensions are in inches unless otherwise noted.

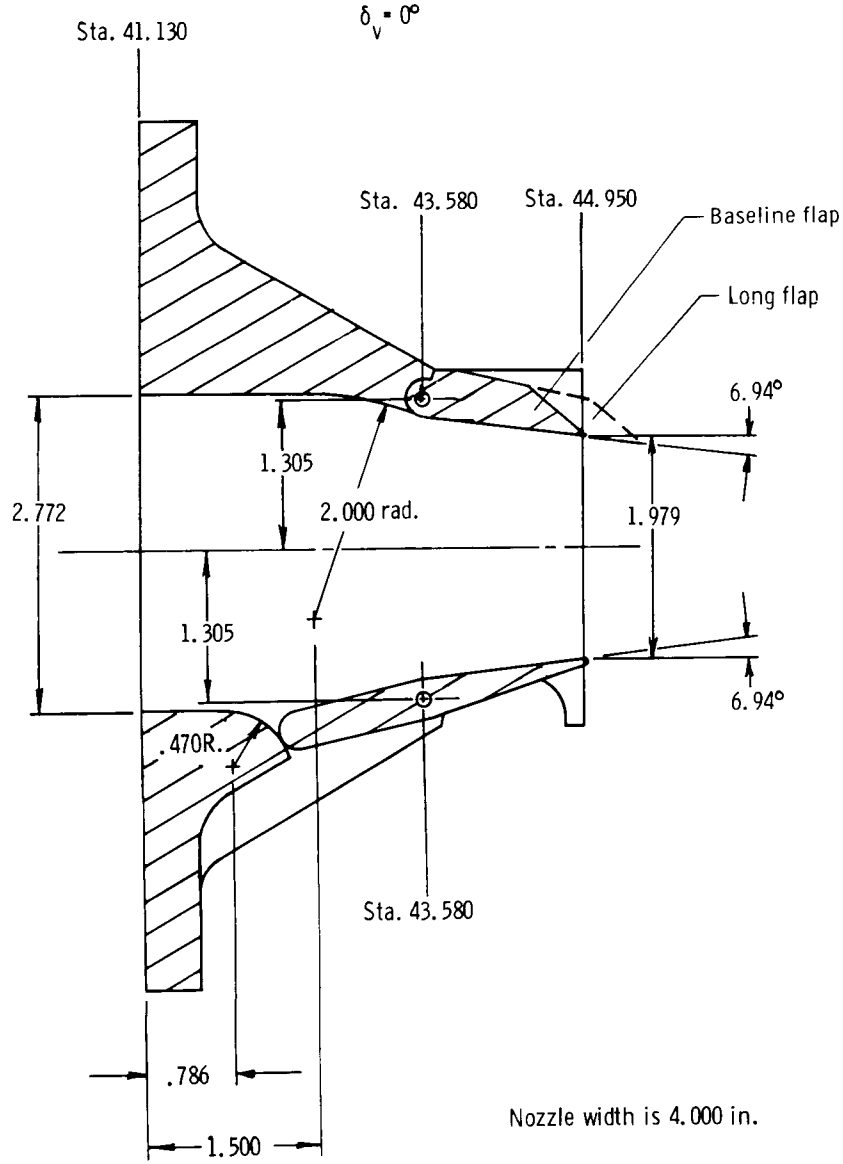

Nozzle width is 4.000 in.

Vectoring configurations

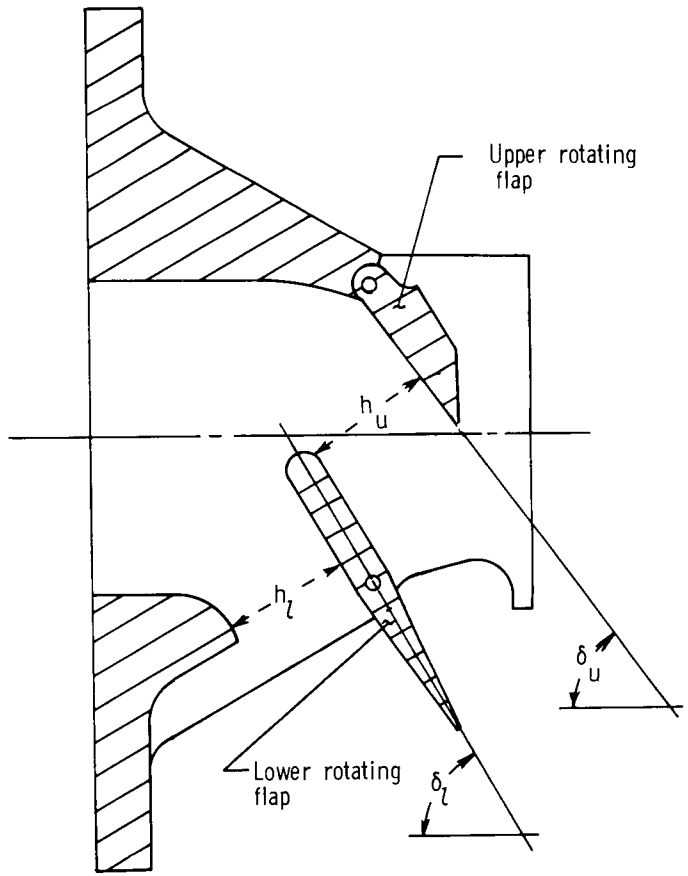

Note: Location of h_u and h_l varies with nominal vector angle δ_v. h_u is located at downstream edge of upper rotating flap on all configurations except δ_v = 60° (configuration shown).

(b) Nozzle geometry.

Figure 3. Continued.

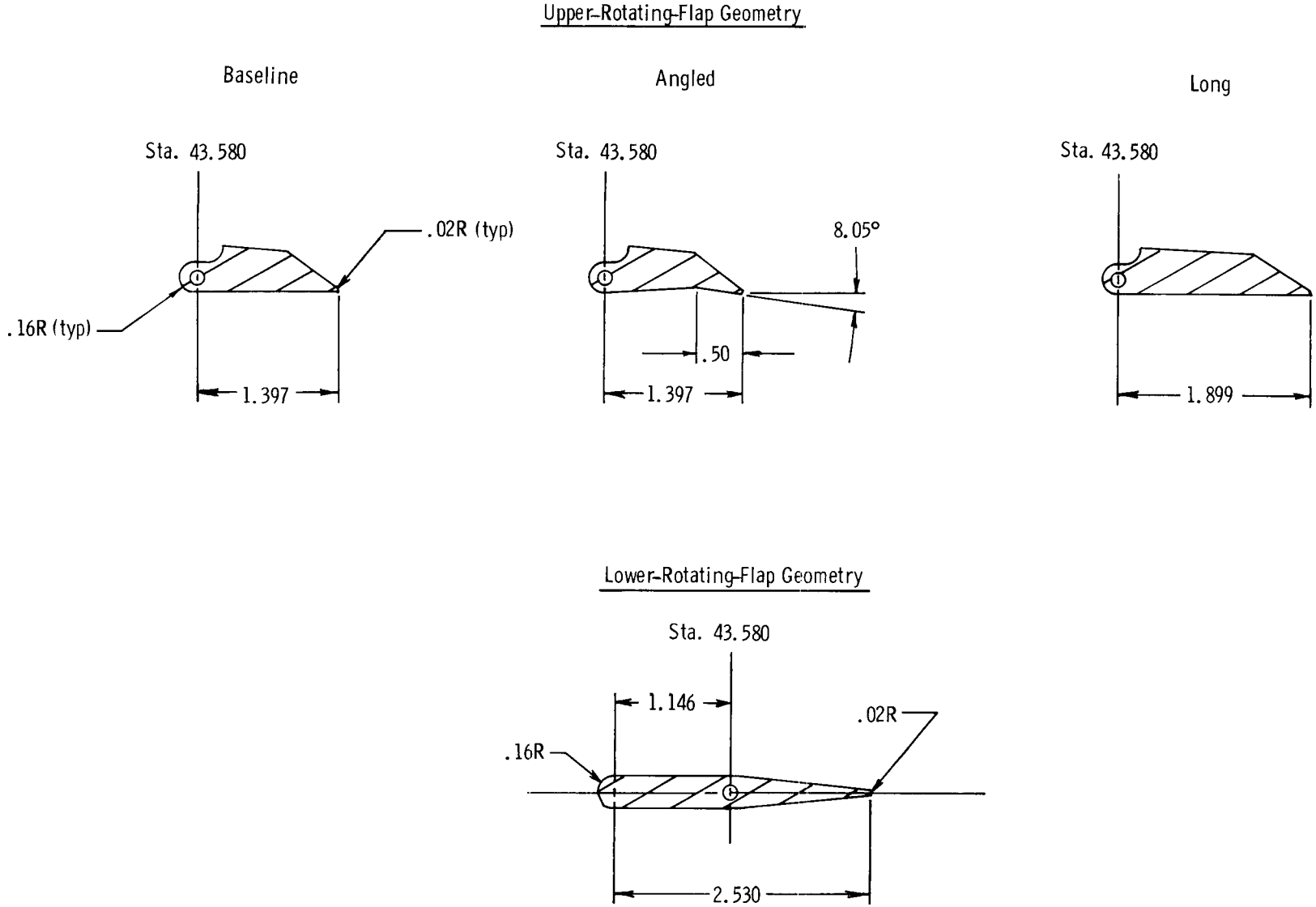

(c) Upper- and lower-rotating-flap geometry.

Figure 3. Continued.

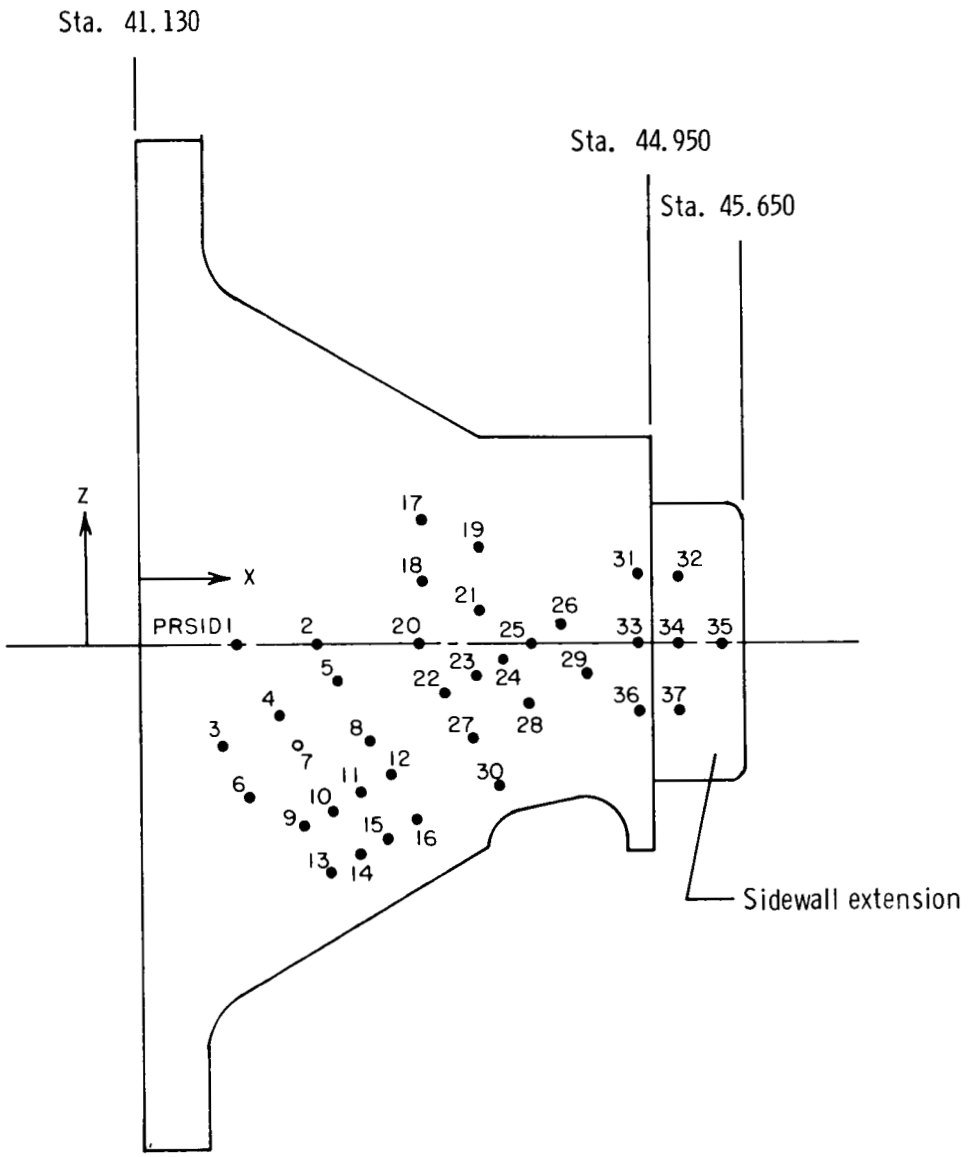

Orifice locations		
Name	x, in.	z, in.
PRSID1	0.75	0.00
2	1.35	0.00
3	0.63	-0.76
4	1.06	-0.53
5	1.50	-0.28
6	0.83	-1.13
7	1.20	-0.75
8	1.74	-0.72
9	1.25	-1.35
10	1.47	-1.23
11	1.69	-1.10
12	1.90	-0.97
13	1.45	-1.70
14	1.67	-1.58
15	1.88	-1.44
16	2.10	-1.31
17	2.13	0.92
18	2.13	0.47
19	2.56	0.71
20	2.10	0.00
21	2.56	0.25
22	2.30	-0.36
23	2.52	-0.24
24	2.74	-0.12
25	2.95	0.00
26	3.19	0.13
27	2.50	-0.71
28	2.94	-0.47
29	3.38	-0.27
30	2.70	-1.08
31	3.75	0.50
32	4.06	0.50
33	3.75	0.00
34	4.06	0.00
35	4.38	0.00
36	3.75	-0.50
37	4.06	-0.50

(d) Pressure orifice locations on sidewall.

Figure 3.- Concluded.

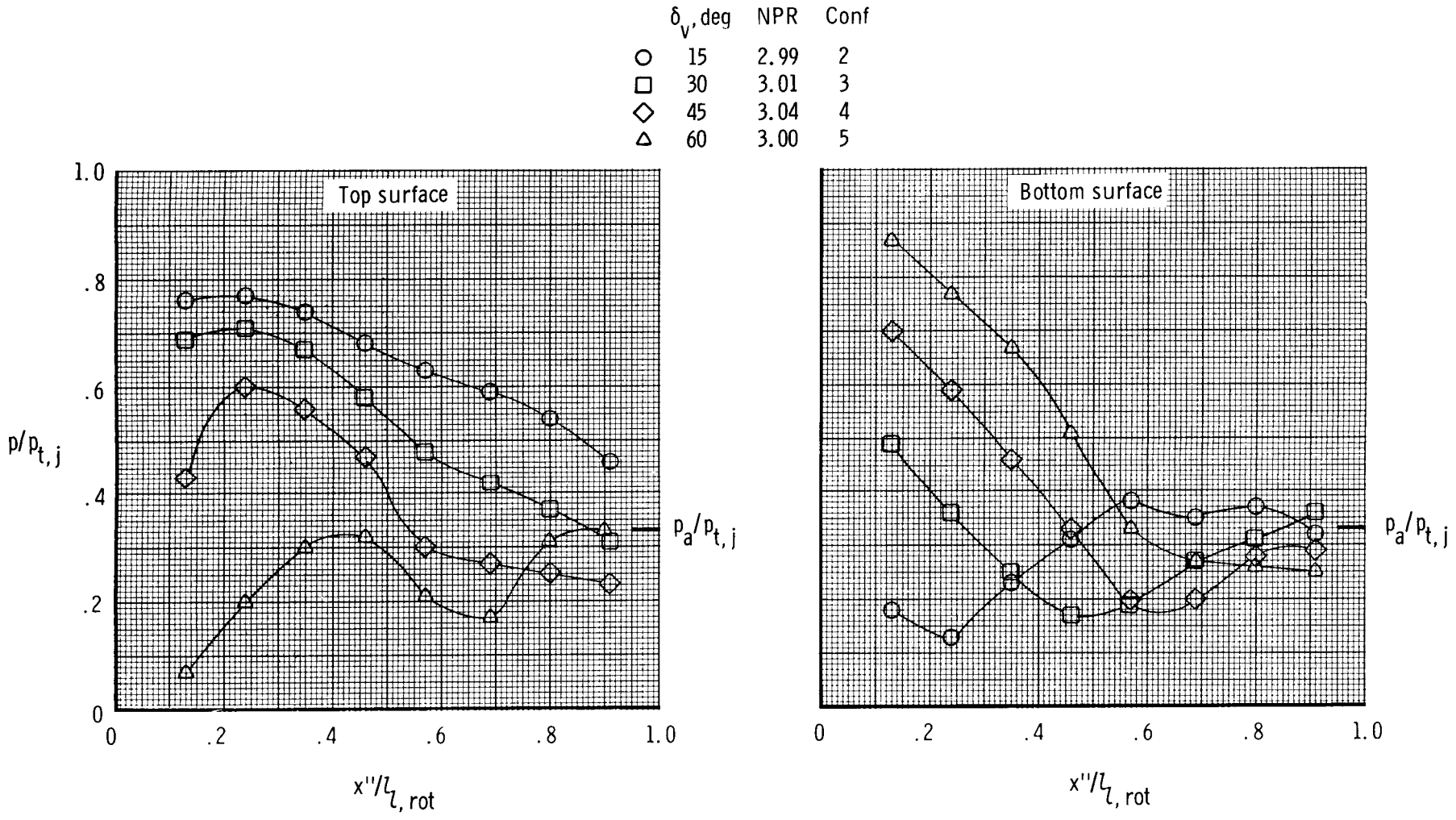

(a) Baseline upper rotating flap.

Figure 4. Effects of vector angle on lower-rotating-flap centerline internal static-pressure distributions.

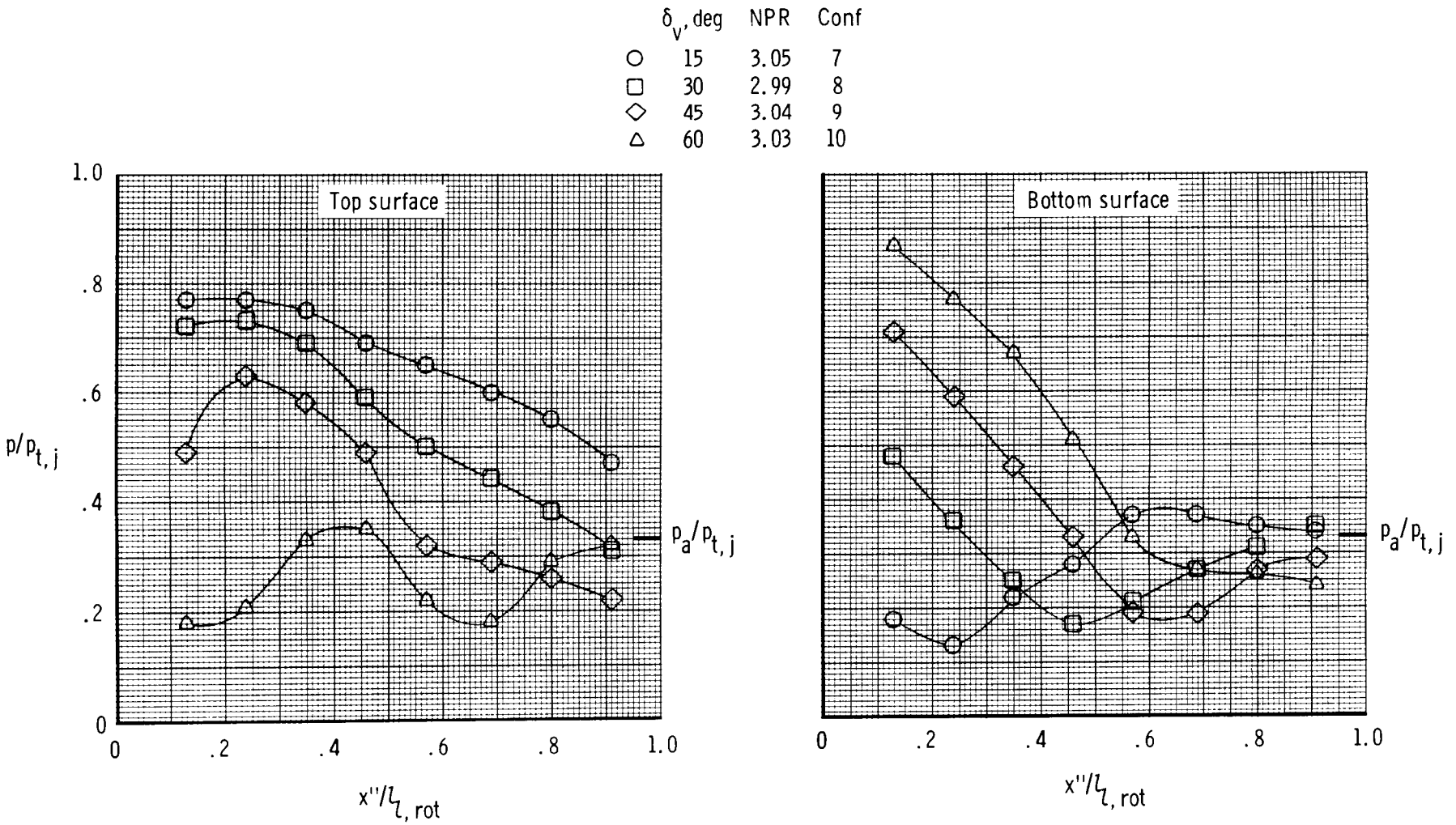

(b) Angled upper rotating flap.

Figure 4. Continued.

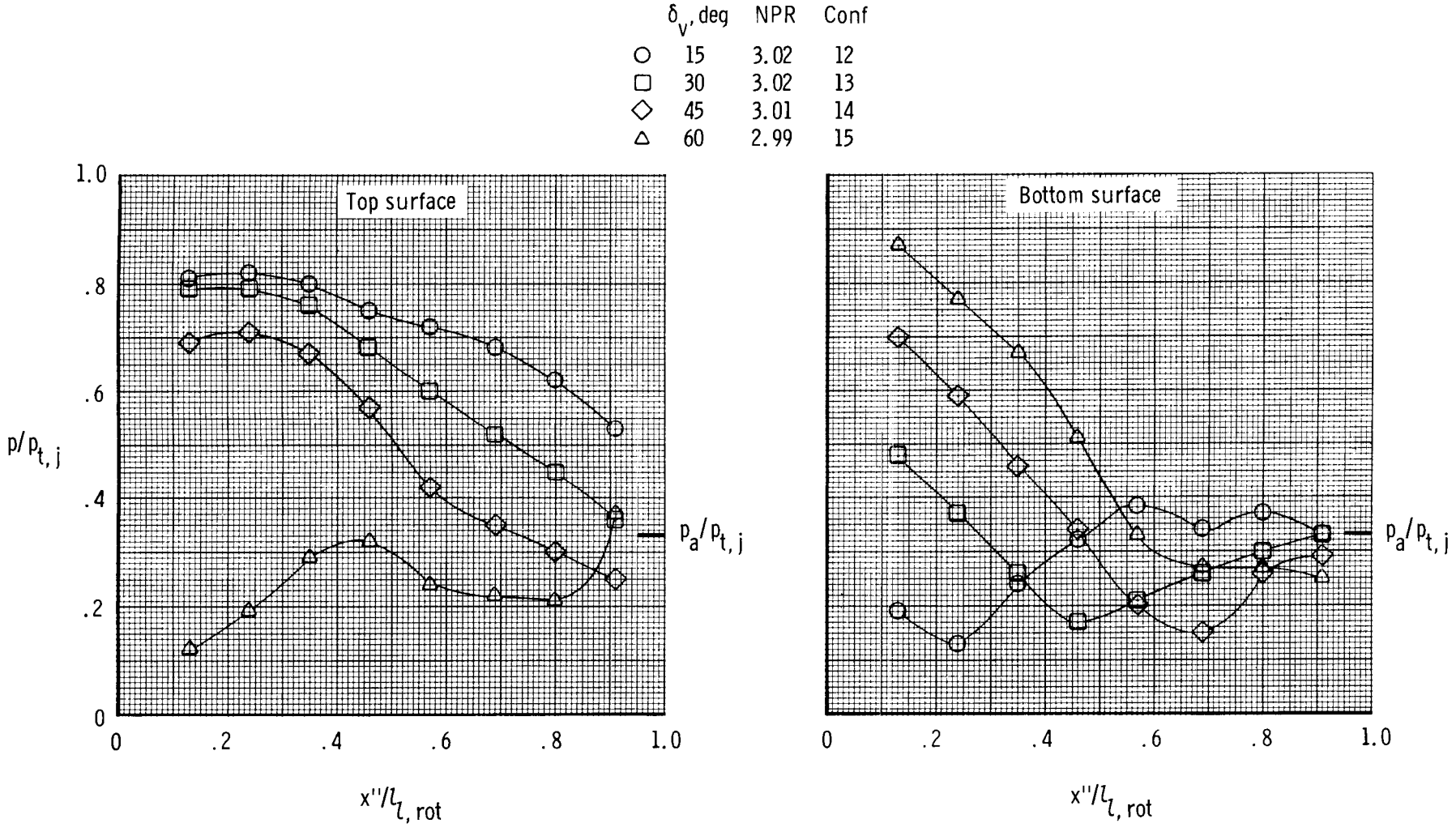

(c) Long upper rotating flap.

Figure 4. Concluded.

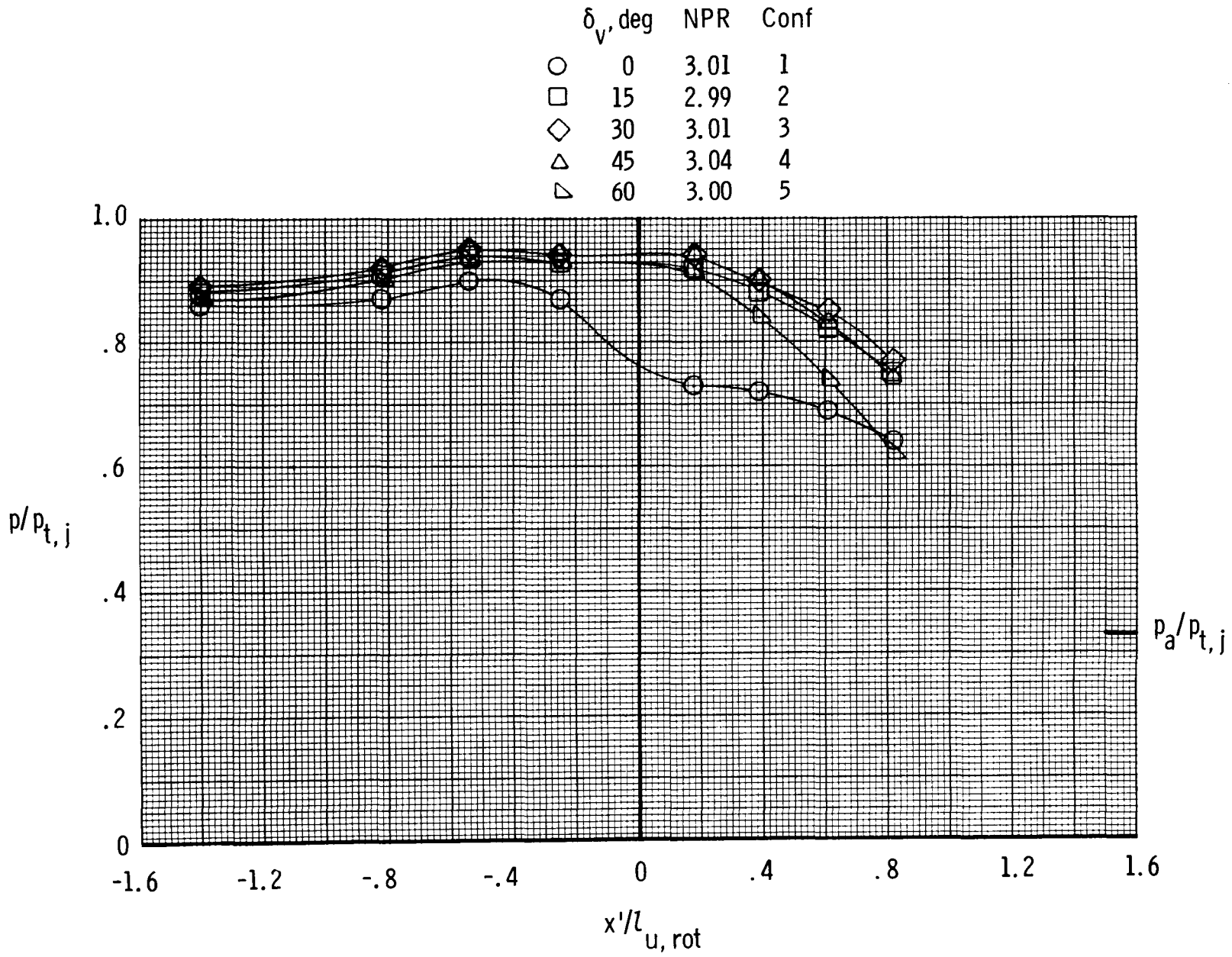

(a) Baseline upper rotating flap.

Figure 5. Effects of vector angle on upper-flap centerline static-pressure distributions.

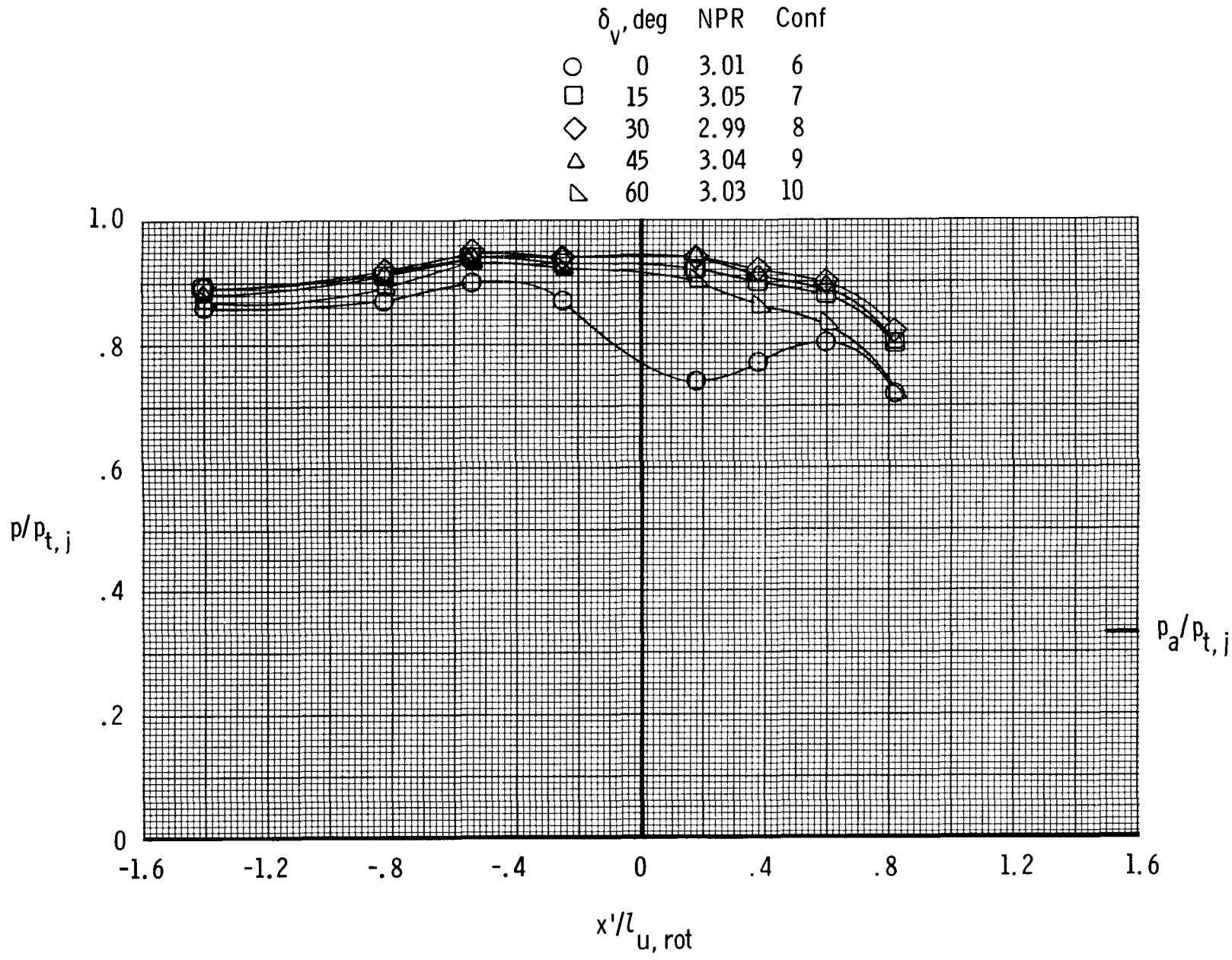

(b) Angled upper rotating flap.

Figure 5. Continued.

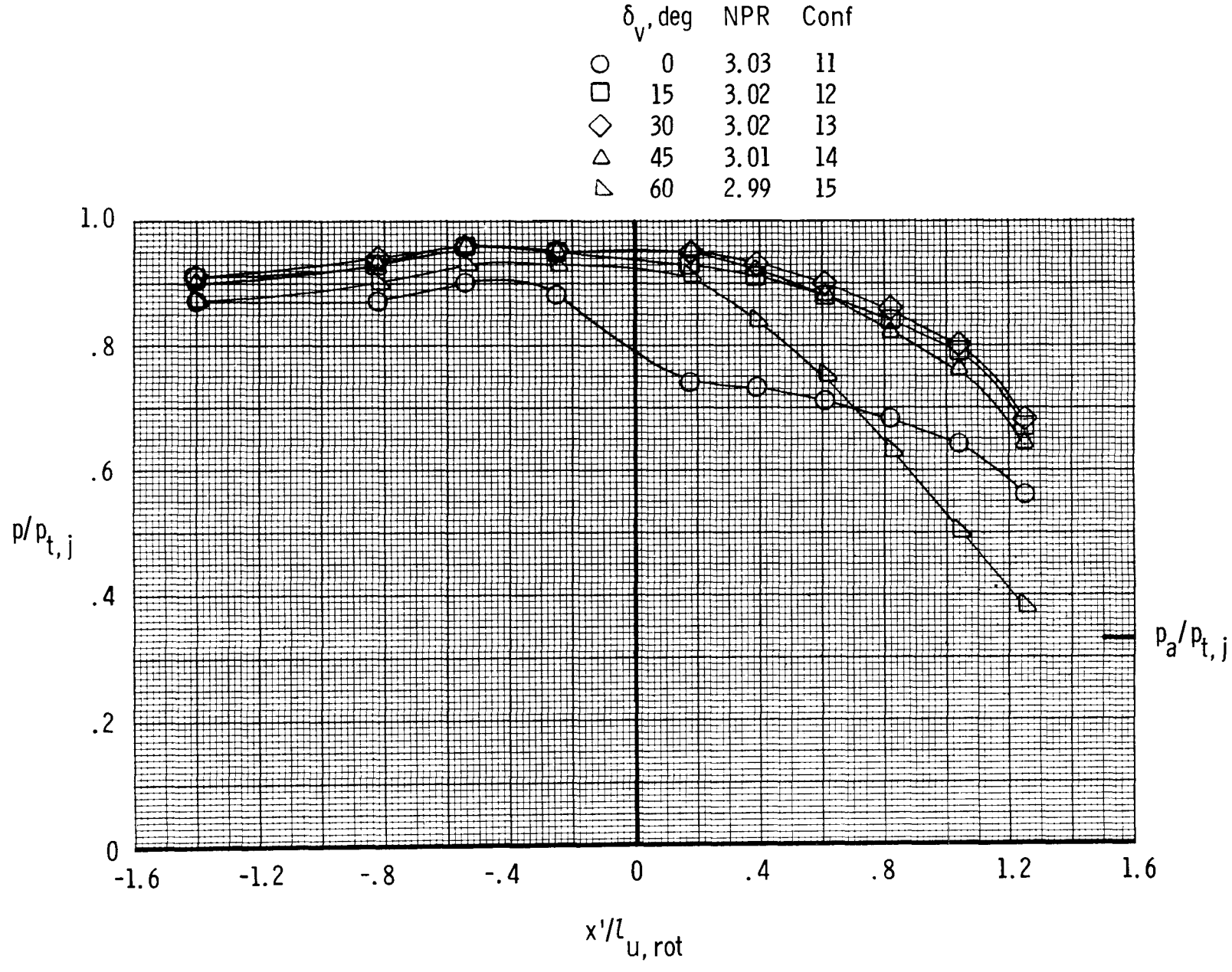

(c) Long upper rotating flap.

Figure 5. Concluded.

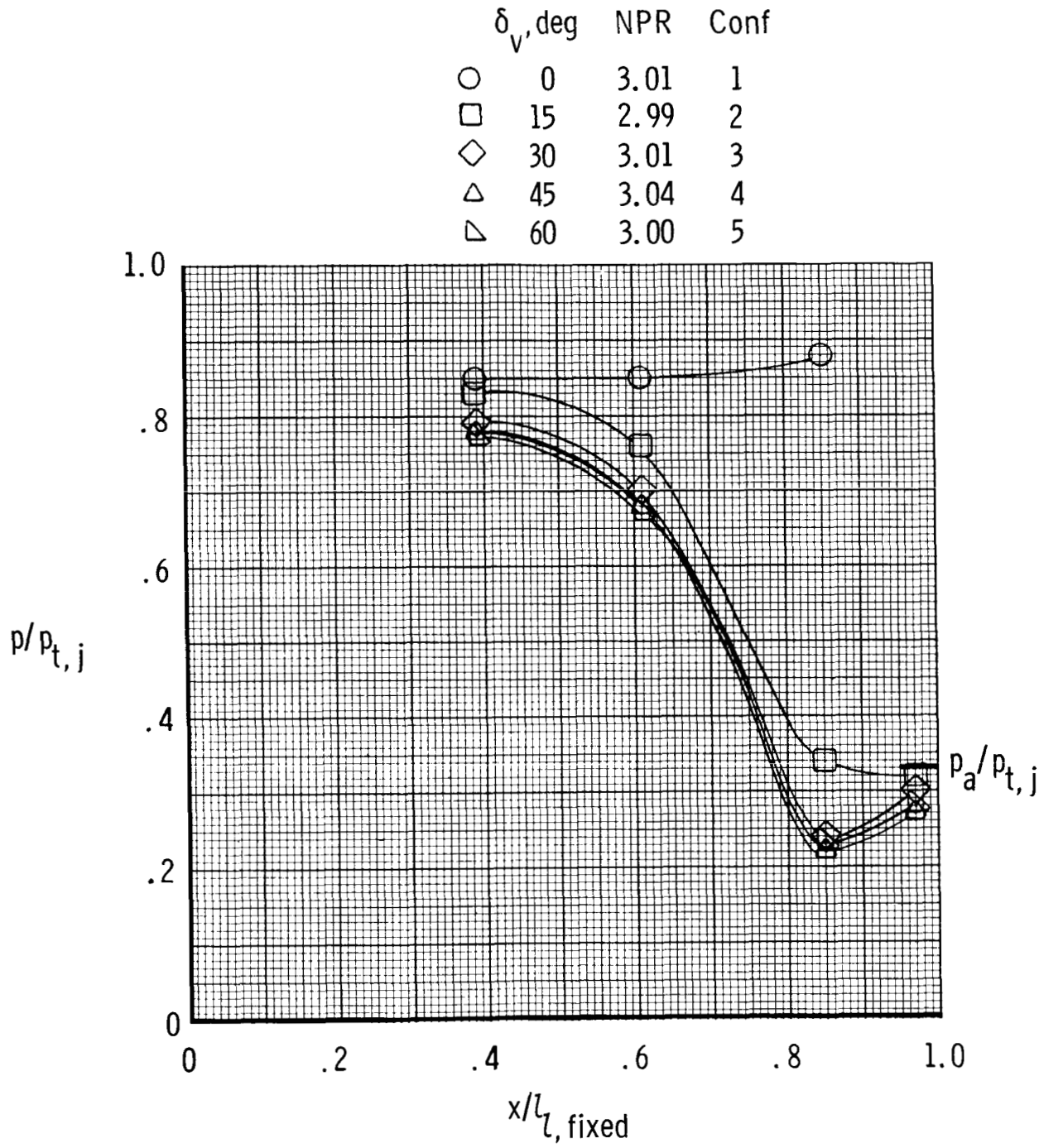

Figure 6. Effects of vector angle on lower-fixed-flap centerline internal static-pressure distributions. Baseline upper rotating flap.

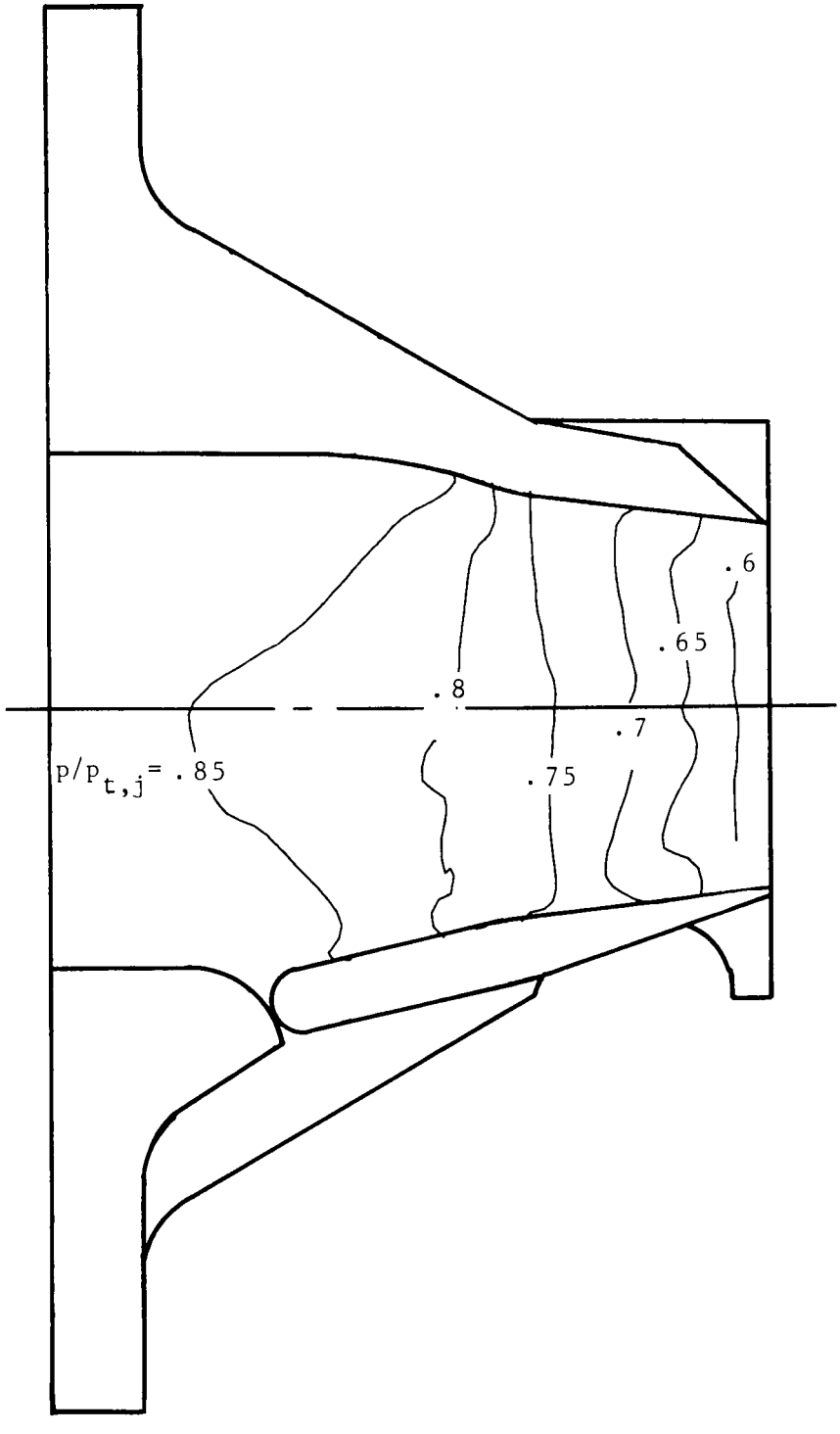

(a) Baseline upper rotating flap with $\delta_v = 0°$.

Figure 7. Sidewall contours of ratio of internal static pressure to jet total pressure for selected configurations. Nominal NPR = 3.0.

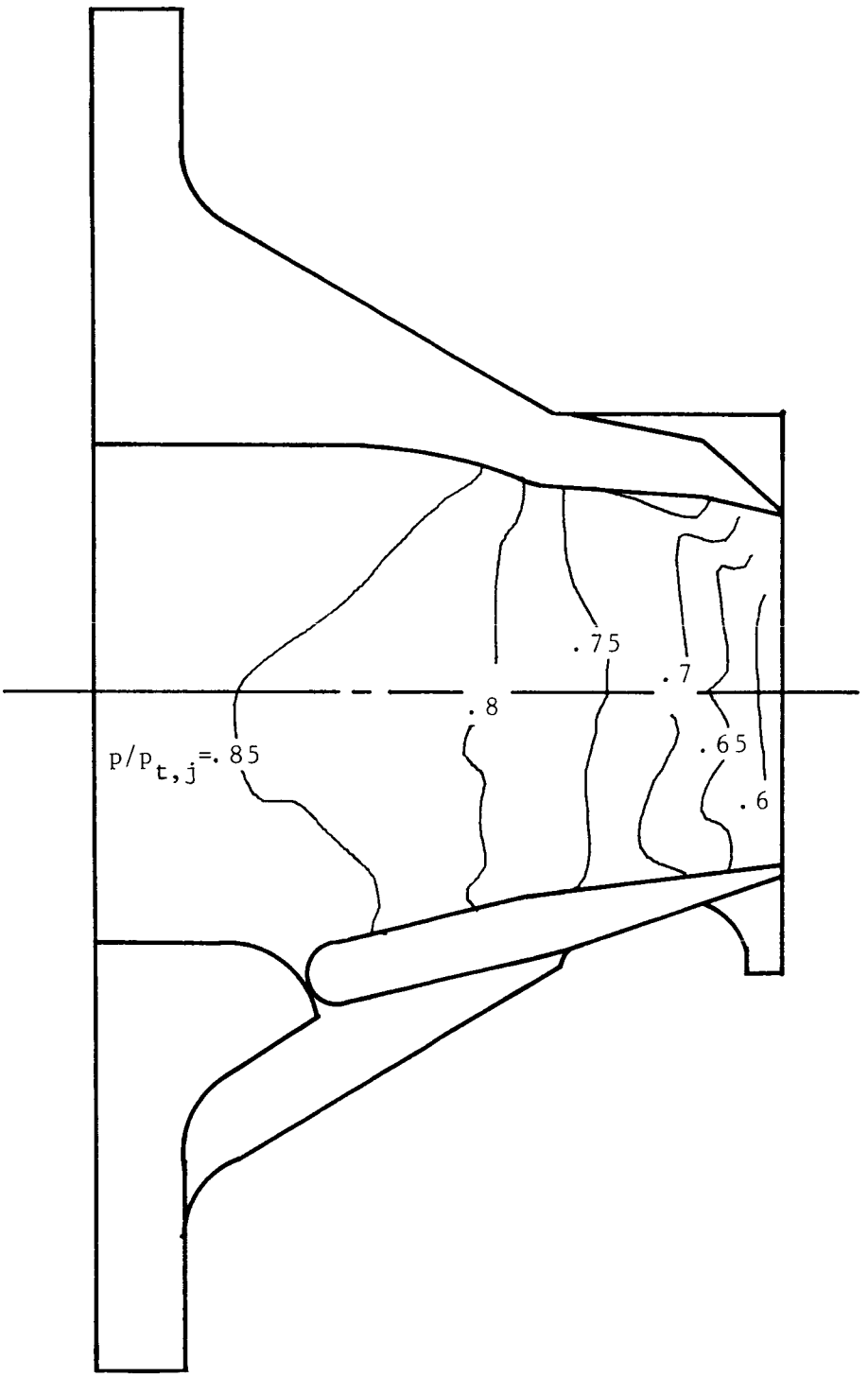

(b) Angled upper rotating flap with $\delta_v = 0°$.

Figure 7. Continued.

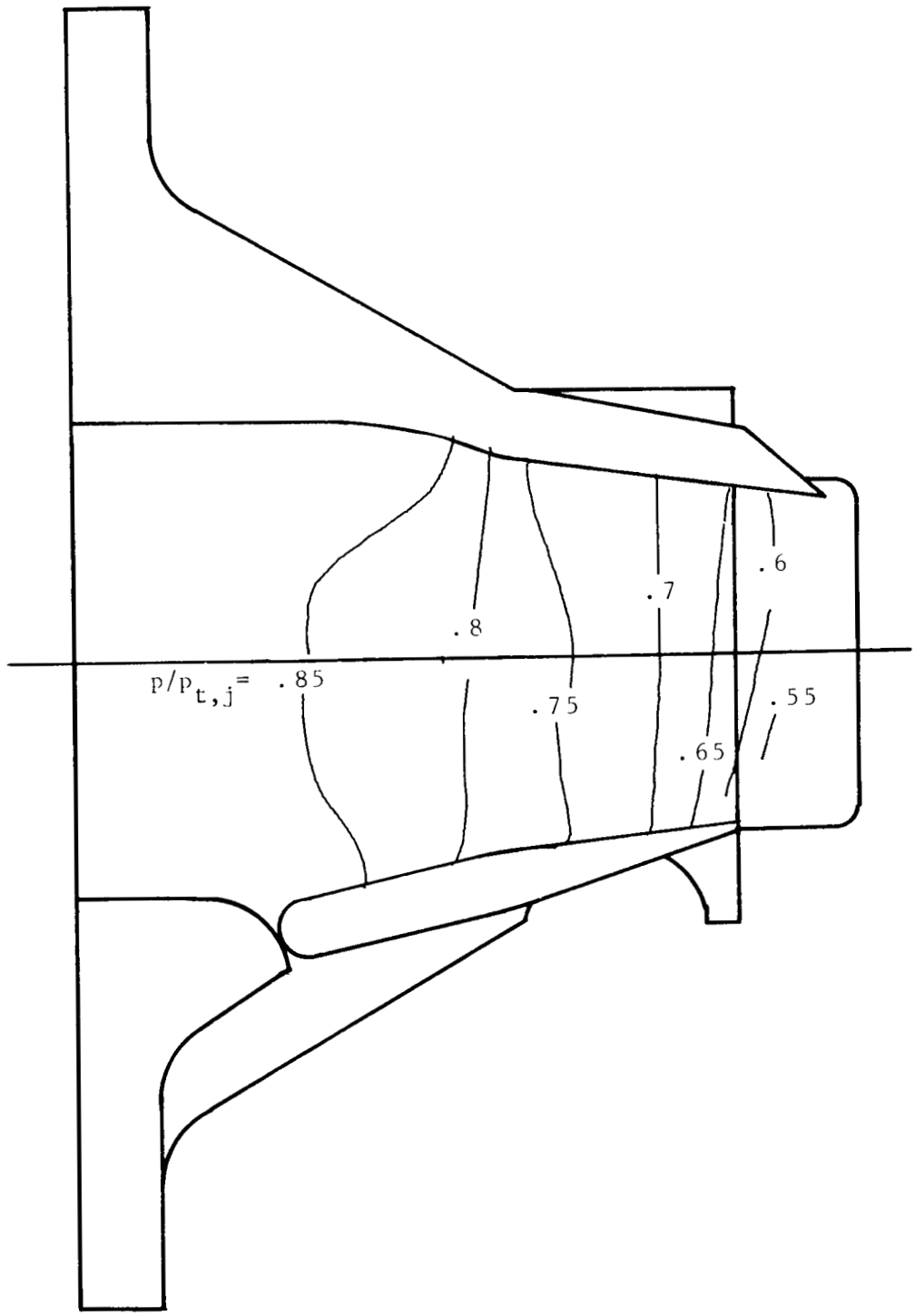

(c) Long upper rotating flap with $\delta_v = 0°$.

Figure 7. Continued.

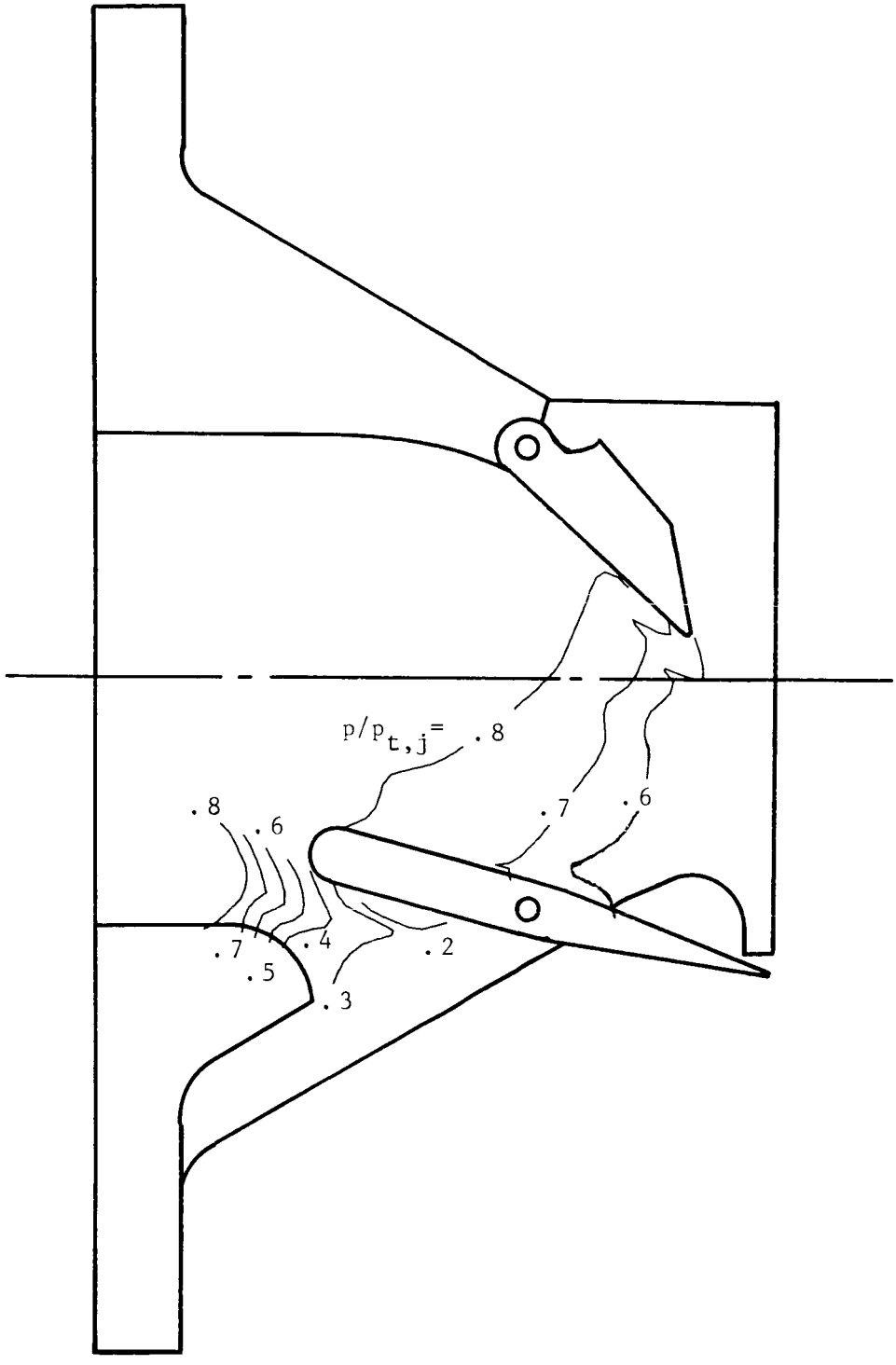

(d) Baseline upper rotating flap with $\delta_v = 15°$.

Figure 7. Continued.

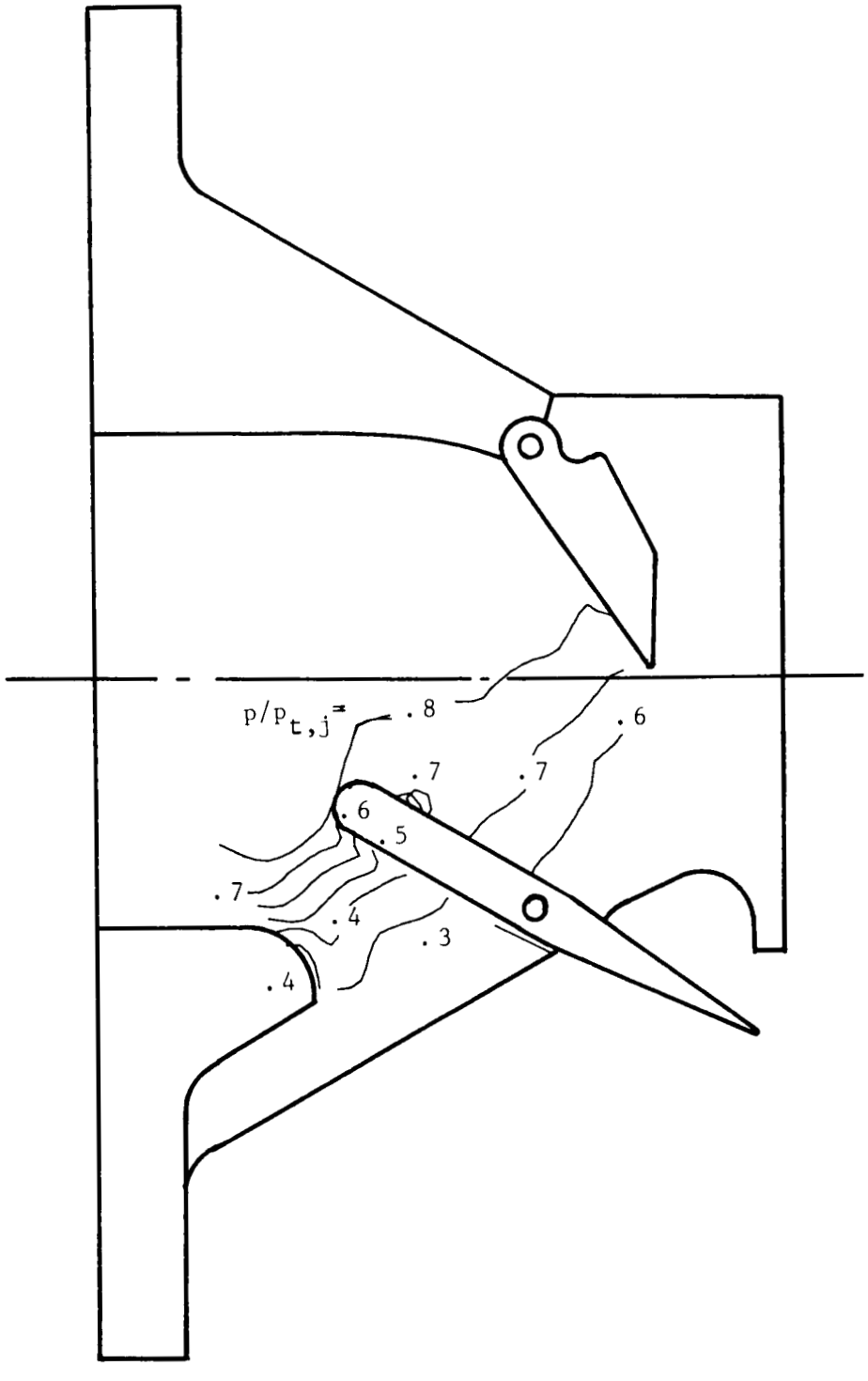

(e) Baseline upper rotating flap with $\delta_v = 30°$.

Figure 7. Continued.

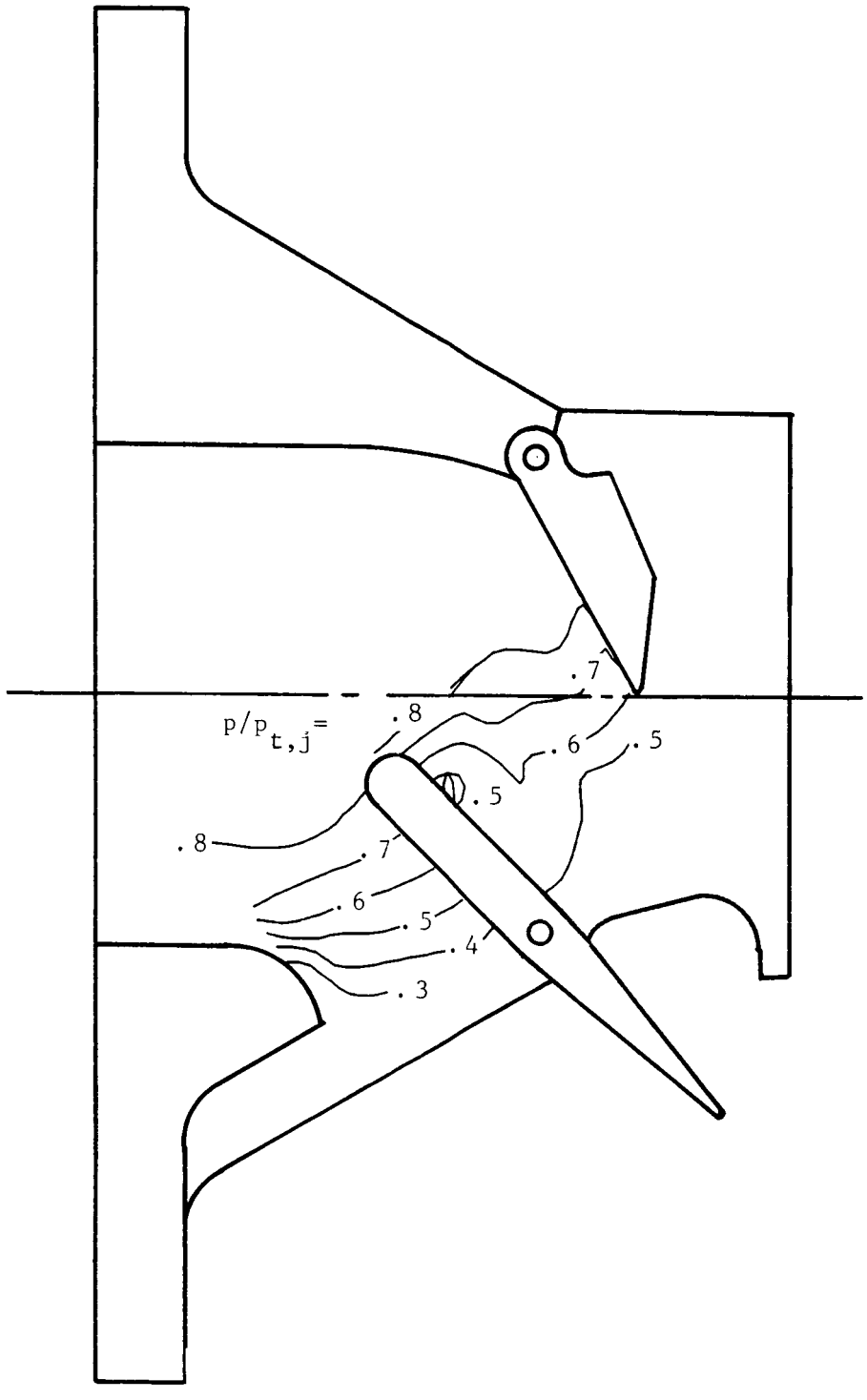

(f) Baseline upper rotating flap with $\delta_v = 45°$.

Figure 7. Continued.

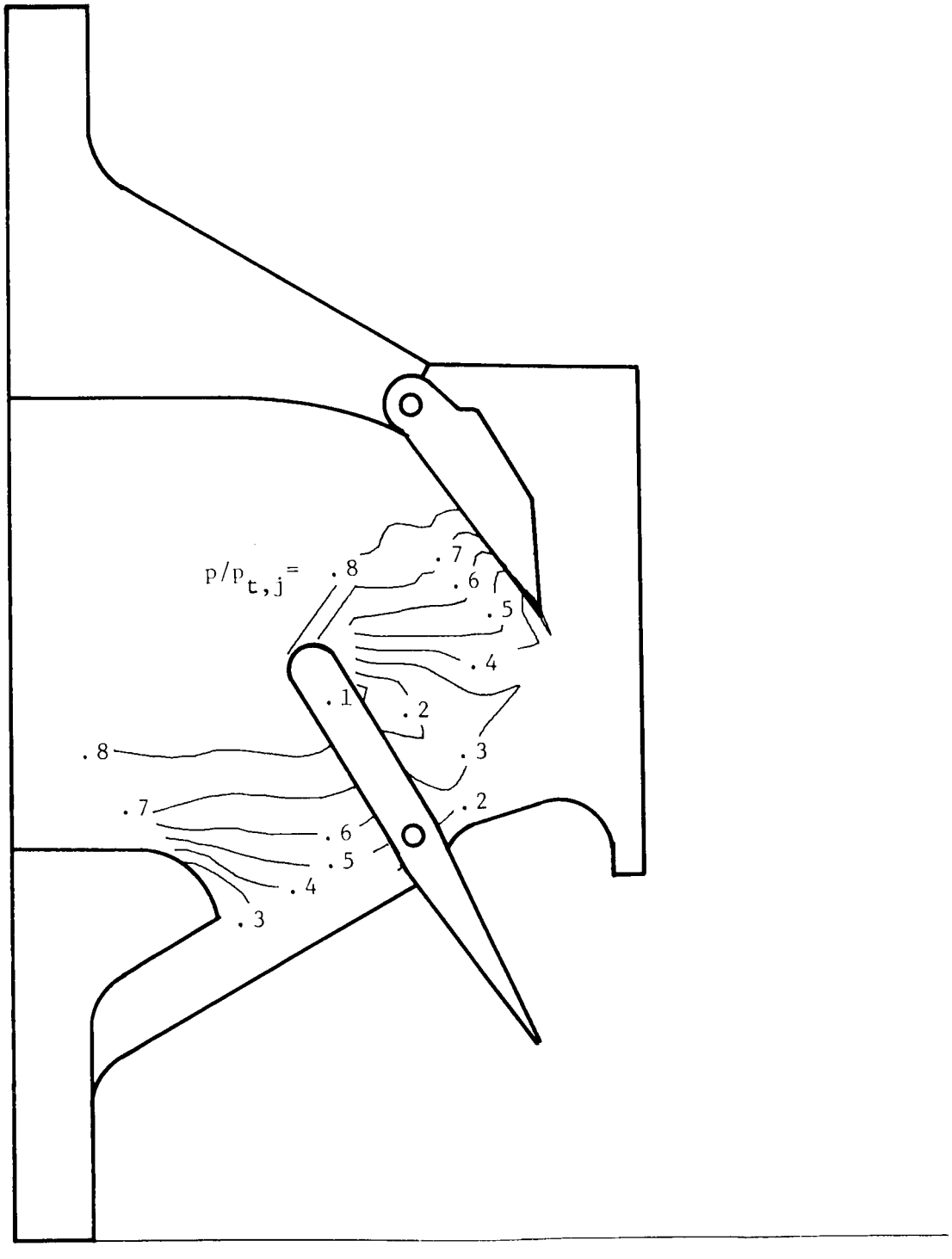

(g) Baseline upper rotating flap with $\delta_v = 60°$.

Figure 7. Concluded.

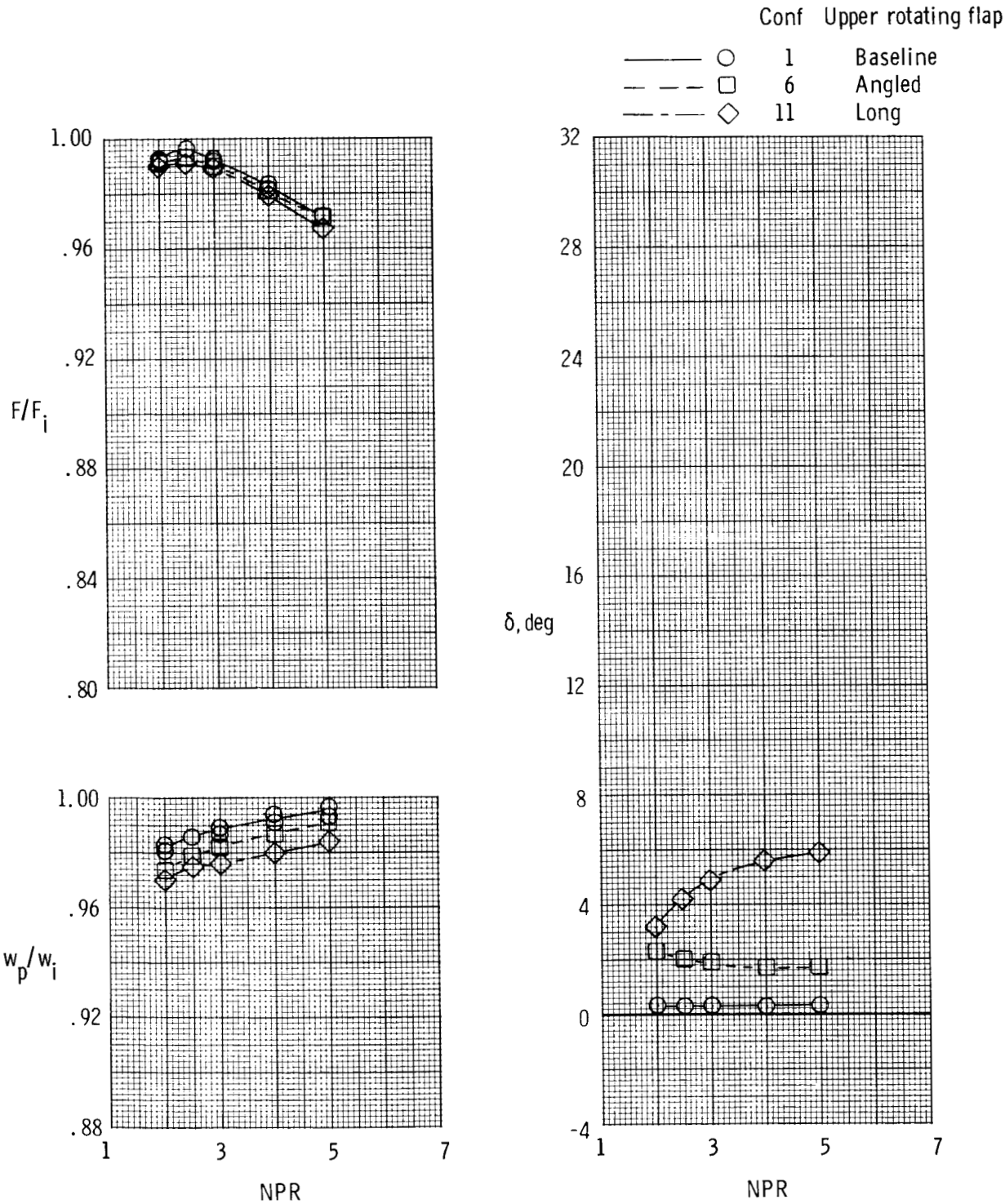

(a) $\delta_v = 0°$.

Figure 8. Effects of upper-rotating-flap configuration on nozzle performance as a function of nozzle pressure ratio. Data without symbols indicate F_r/F_i.

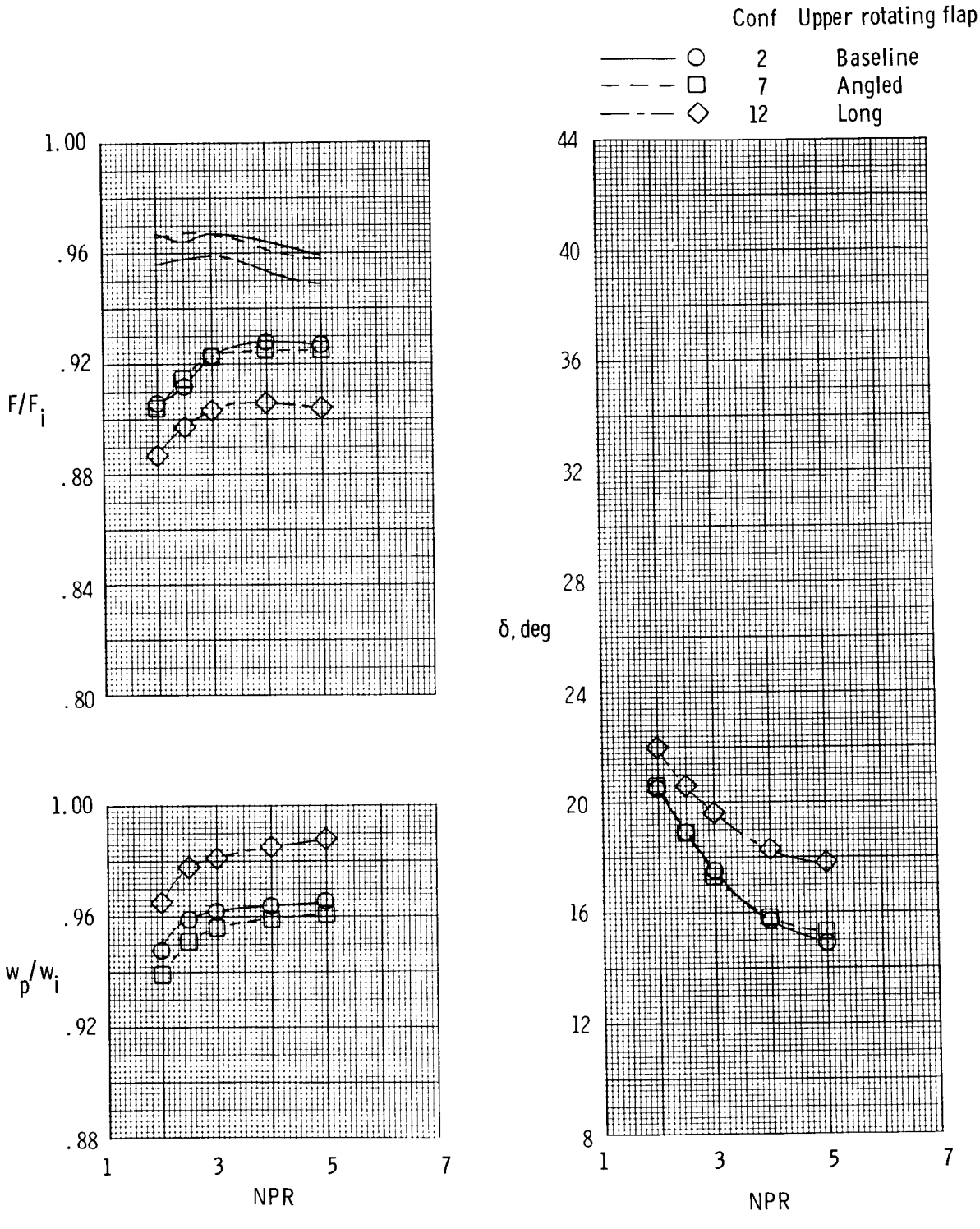

(b) $\delta_v = 15°$.

Figure 8. Continued.

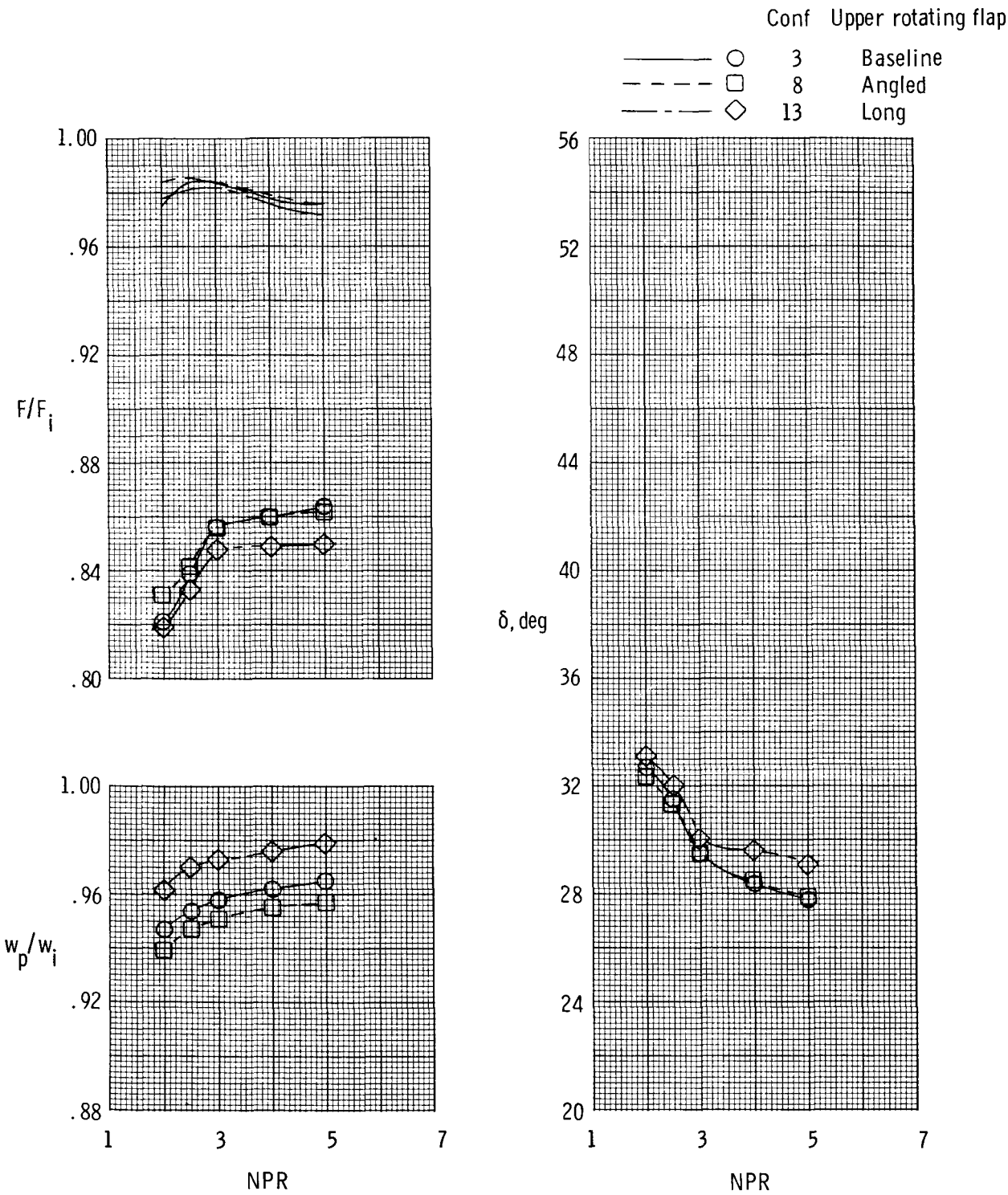

(c) $\delta_v = 30°$.

Figure 8. Continued.

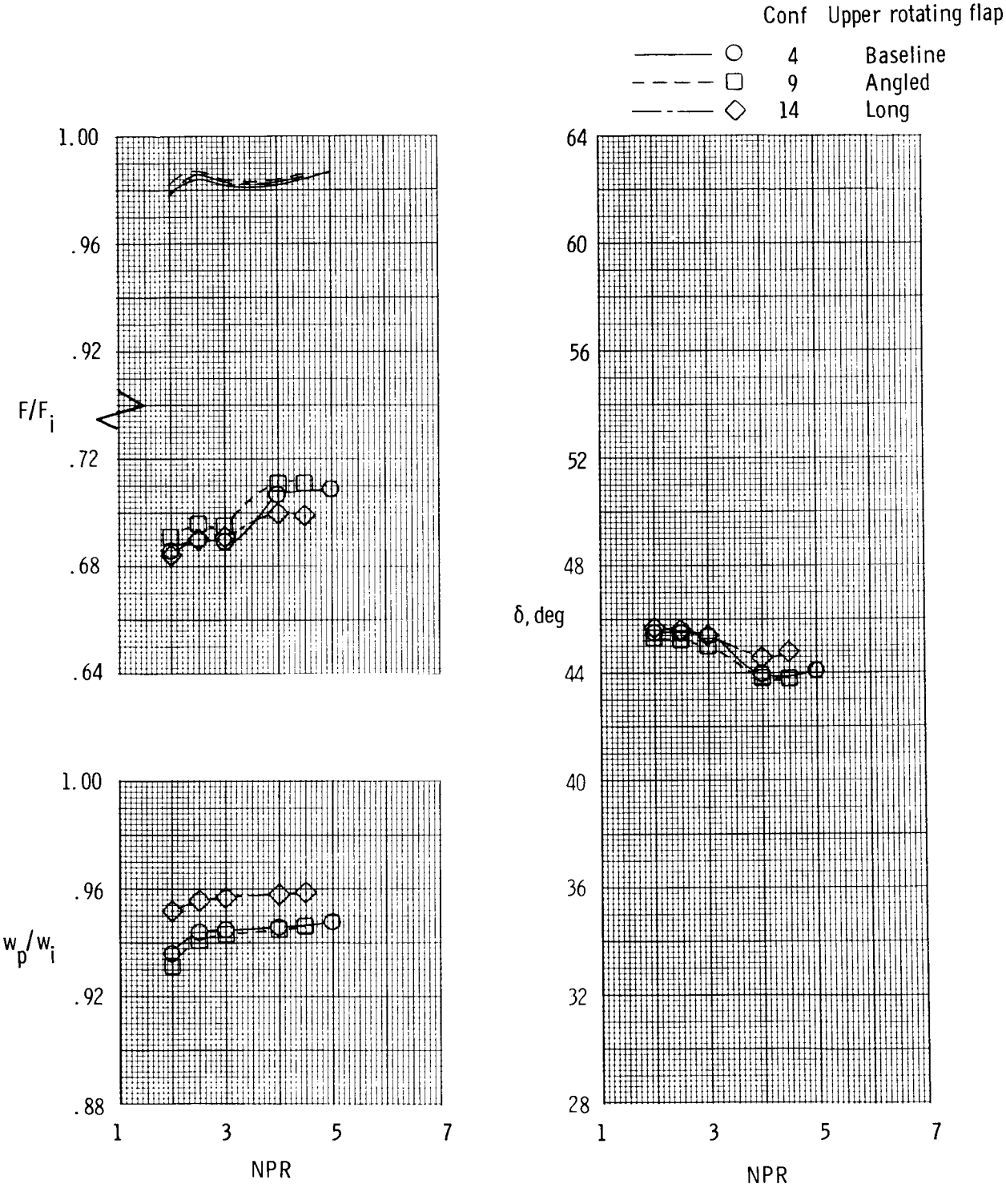

(d) $\delta_v = 45°$.

Figure 8. Continued.

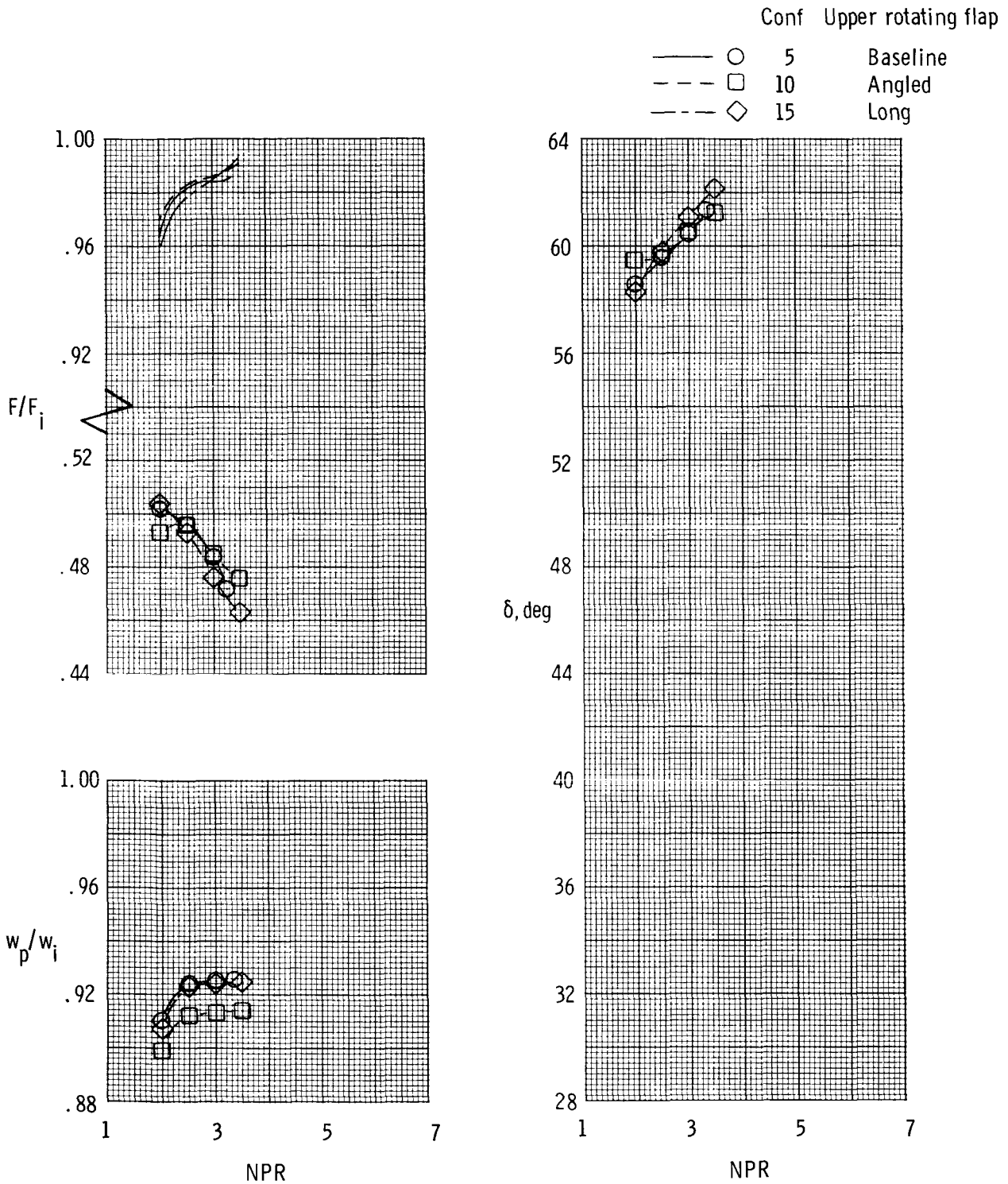

(e) $\delta_v = 60°$.

Figure 8. Concluded.

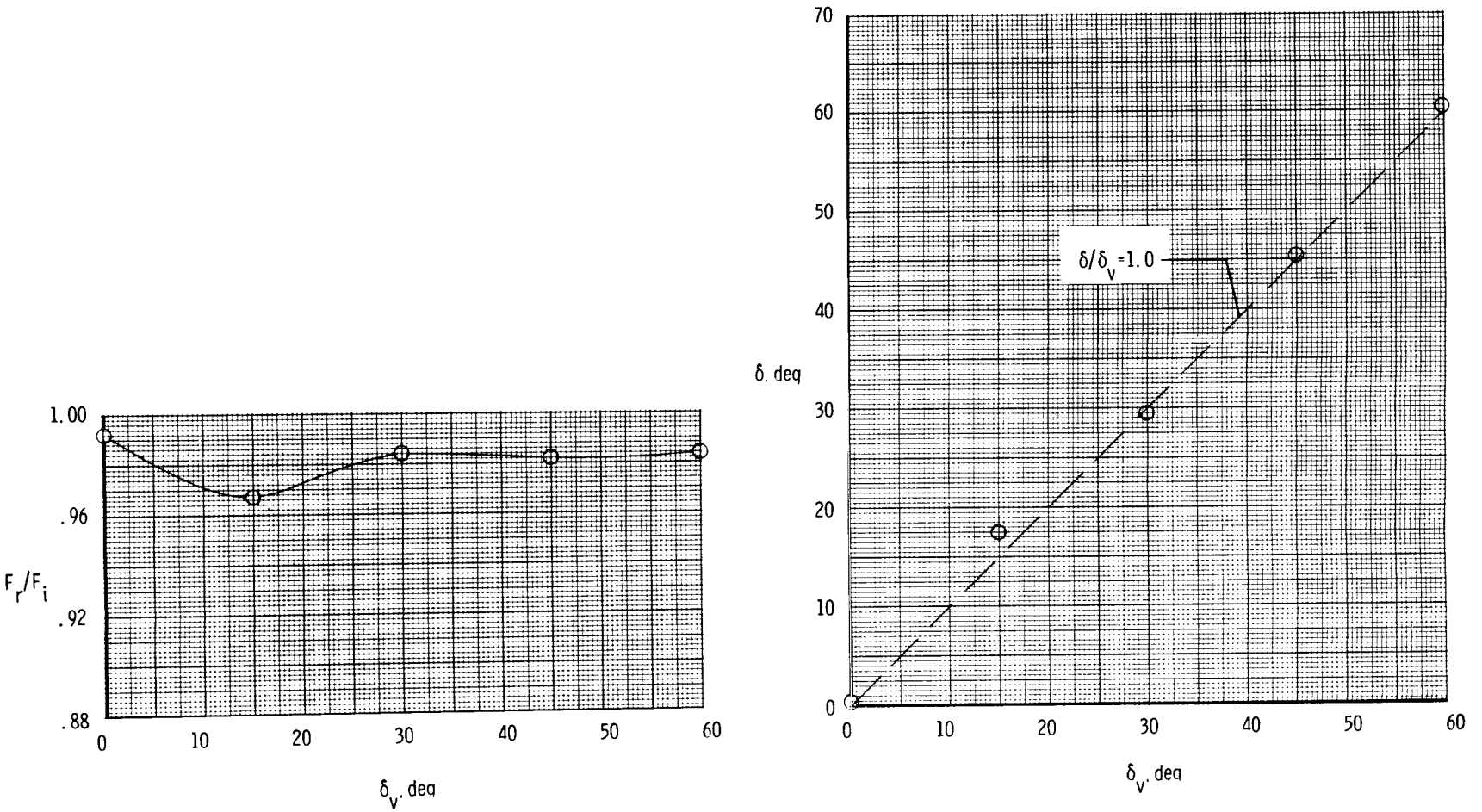

Figure 9. Effects of design vector angle on resultant gross thrust ratio and thrust-vector angle. Baseline upper rotating flap; NPR = 3.0.

1. Report No.	2. Government Accession No.	3. Recipient's Catalog No.
NASA TP-2391		

4. Title and Subtitle	5. Report Date
STATIC INTERNAL PERFORMANCE OF A TWO-DIMENSIONAL CONVERGENT NOZZLE WITH THRUST-VECTORING CAPABILITY UP TO 60°	February 1985
	6. Performing Organization Code: 505-43-90-07
7. Author(s): Laurence D. Leavitt	8. Performing Organization Report No.: L-15837
9. Performing Organization Name and Address: NASA Langley Research Center, Hampton, VA 23665	10. Work Unit No.
	11. Contract or Grant No.
12. Sponsoring Agency Name and Address: National Aeronautics and Space Administration, Washington, DC 20546	13. Type of Report and Period Covered: Technical Paper
	14. Sponsoring Agency Code

15. Supplementary Notes

16. Abstract

An investigation has been conducted at wind-off conditions in the static-test facility of the Langley 16-Foot Transonic Tunnel to determine the internal performance characteristics of a two-dimensional convergent nozzle with a thrust-vectoring capability up to 60°. Vectoring was accomplished by a downward rotation of a hinged upper convergent flap and a corresponding rotation of a center-pivoted lower convergent flap. The effects of geometric thrust-vector angle and upper-rotating-flap geometry on internal nozzle performance characteristics were investigated. Nozzle pressure ratio was varied from 1.0 (jet off) to approximately 5.0.

17. Key Words (Suggested by Authors(s))
Nonaxisymmetric nozzles
Two-dimensional nozzles
Convergent nozzles
Internal performance
Thrust vectoring

18. Distribution Statement
Unclassified—Unlimited

Subject Category 02

19. Security Classif.(of this report)	20. Security Classif.(of this page)	21. No. of Pages	22. Price
Unclassified	Unclassified	68	A04

For sale by the National Technical Information Service, Springfield, Virginia 22161

NASA-Langley, 1985

National Aeronautics and Space Administration

Washington, D.C.
20546

Official Business
Penalty for Private Use, $300

THIRD-CLASS BULK RATE

Postage and Fees Paid
National Aeronautics and Space Administration
NASA-451

3 2 1U,A, 850131 S00161DS
DEPT OF THE AIR FORCE
ARNOLD ENG DEVELOPMENT CENTER(AFSC)
ATTN: LIBRARY/DOCUMENTS
ARNOLD AF STA TN 37389

NASA

POSTMASTER: If Undeliverable (Section 158 Postal Manual) Do Not Return